Supporting Information For

A Syn Outer-Sphere Oxidative Addition: The Reaction Mechanism in Pd/Senphos-Catalyzed Carboboration of 1,3-Enynes

Ziyong Wang,[a] Walid Lamine,[b] Karinne Miqueu,*[b] Shih-Yuan Liu*[a,b]

[a]Department of Chemistry, Boston College, Chestnut Hill, Massachusetts 02467-3860, United States
[b]Université de Pau et des Pays de l'Adour, E2S UPPA, CNRS, IPREM UMR 5254, Hélioparc, 2 avenue P. Angot, 64053 Pau cedex 09, France

1. General Information

All oxygen- and moisture-sensitive manipulations were carried out under an inert atmosphere using either standard Schlenk techniques or a glove box. Unless otherwise noted, all reagents were obtained from commercial sources and used as received. Bulk volumes of diethyl ether, dichloromethane, pentane, toluene and tetrahydrofuran were passed through an alumina column and dispensed from a solvent purification system under argon.

^{1}H, ^{13}C, ^{11}B, and ^{19}F NMR spectra were measured on Varian 400, 500 or 600 MHz spectrometers or Inova 500 MHz spectrometer at the Boston College nuclear magnetic resonance facility. Data are reported as follows: chemical shift, integration, multiplicity (s = singlet, d = doublet, t = triplet, q = quartet, br = broad, m = multiplet), and coupling constant (Hz). ^{1}H and ^{13}C spectra were internally referenced to residual solvent peaks (^{1}H $CDCl_3$: δ = 7.26 ppm, ^{13}C $CDCl_3$: δ = 77.16 ppm, ^{1}H toluene-d_8: δ = 2.09 ppm); ^{11}B spectra were externally referenced to a standard of $BF_3 \bullet Et_2O$ (δ = 0.0 ppm), and ^{19}F spectra were referenced to of α,α,α-trifluorotoluene (δ = −63.7 ppm). In ^{13}C NMR analysis, peaks for carbon atoms adjacent to a boron center were generally not observed owing to quadrupolar broadening.

$CDCl_3$ was purchased from Cambridge Isotope Laboratories and was passed through K_2CO_3 plug and then distilled over P_2O_5 under N_2 and stored over activated 4Å molecular sieves prior to use. Toluene-d_8 was purchased from Cambridge Isotope Laboratories and was distilled over CaH_2 and then degassed through freeze-pump-thaw cycles. All work-up and purification procedures were carried out with reagent grade solvents (purchased from Fisher Scientific) in air unless otherwise noted.

All IR spectra were measured on a Bruker Alpha-P FT-IR equipped with a single crystal diamond ATR module, and values are reported in cm^{-1}.

High-resolution mass spectrometry (HRMS) data were generated in Boston College facilities using direct analysis in real-time (DART) on a JEOL AccuTOF DART spectrometer.

2. ^{31}P NMR Experiments (Scheme 3)

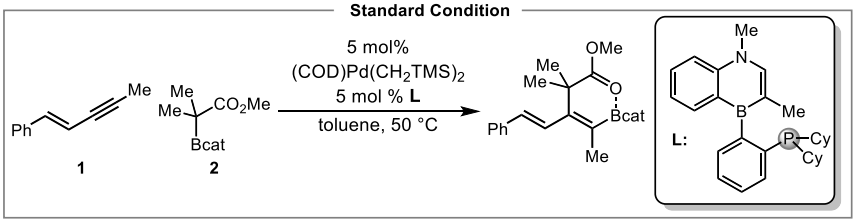

1) In a nitrogen-filled glovebox, an oven-dried vial (4 mL) was sequentially charged with (COD)Pd(CH_2TMS)$_2$ (7.8 mg, 20 μmol), **L** (8.6 mg, 20 μmol), and toluene (500 μL). The solution was allowed to stir at room temperature for 10 min and the resulting green solution was transferred to an oven-dried J-Young tube. Then, the J-Young tube was tightly capped with the Teflon plug and taken out of the glove box. A ^{31}P NMR spectrum was acquired in the NMR spectrometer preheated at 50 °C, which was labeled as **Spectrum A**.
2) In a nitrogen-filled glovebox, an oven-dried vial (4 mL) was sequentially charged with (COD)Pd(CH_2TMS)$_2$ (7.8 mg, 20 μmol), **L** (8.6 mg, 20 μmol), and toluene (100 μL). The solution was allowed to stir at room temperature for 10 min before adding a solution of **1** (56.9 mg, 0.40 mmol, 20.0 equiv.) in toluene (400 μL). The resulting yellow solution was allowed to stir for another 5 min before being transferred to an oven-dried J-Young tube. The J-Young tube was tightly capped with the Teflon plug, taken out of the glove box, and the ^{31}P NMR spectrum was acquired in the NMR spectrometer preheated at 50 °C, which was labeled as **Spectrum B**.
3) In a nitrogen-filled glovebox, an oven-dried vial (4 mL) was sequentially charged with (COD)Pd(CH_2TMS)$_2$ (7.8 mg, 20 μmol), **L** (8.6 mg, 20 μmol), and toluene (100 μL). The solution was allowed to stir at room temperature for 10 min before adding a solution of **2** (176 mg, 0.800 mmol, 40.0 equiv.) in toluene (400.0 μL). The resulting yellow solution was allowed to stir for another 5 min before being transferred to an oven-dried J-Young tube. Then, the J-Young tube was tightly capped with the Teflon plug, taken out of the glove box, and the ^{31}P NMR spectrum was acquired in the NMR spectrometer preheated at 50 °C, which was labeled as **Spectrum C**.
4) In a nitrogen-filled glovebox, an oven-dried vial (4 mL) was sequentially charged with (COD)Pd(CH_2TMS)$_2$ (7.8 mg, 20 μmol), **L** (8.6 mg, 20 μmol), and toluene (100 μL). The solution was allowed to stir at room temperature for 10 min before adding a solution of **1** (57 mg, 0.40 mmol, 20 equiv.) in toluene (100 μL). The resulting yellow solution was allowed to stir for another 5 min before adding a solution of **2** (176 mg, 0.800 mmol, 40.0 equiv.) in toluene (150 μL). The reaction mixture was transferred to an oven-dried J-Young tube, and the ^{31}P NMR spectrum was acquired in the NMR spectrometer preheated at 50 °C using a pre-acquisition delay in array mode for the length of the experiment. The spectrum of an actively running reaction is illustrated as **Spectrum D**.

3. Initial-rate Kinetic Study (Scheme 4)

We determined the kinetic orders in [**1**], [**2**] and [**Pd/L$_{total}$**] via initial-rate kinetics observed by ^{1}H NMR spectroscopy analysis.

3.1 Procedure for Reaction Order Determination for Enyne **1**

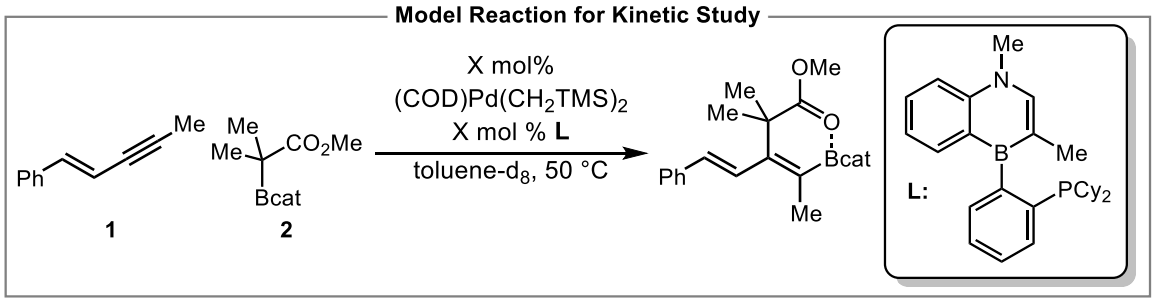

In a nitrogen-filled glovebox, (COD)Pd(CH$_2$TMS)$_2$ (38.9 mg, 0.100 mmol), **L** (43.0 mg, 0.100 mmol) was dissolved in toluene-d$_8$ to prepare **Stock Solution A** (0.500 mL, 0.200 M). Enyne **1** (379 mg, 2.67 mmol) was dissolved in toluene-d$_8$ to prepare **Stock Solution B** (0.500 mL, 5.34 M). C-boron enolate **2** (880 mg, 4.00 mmol) was dissolved in toluene-d$_8$ to prepare **Stock Solution C** (1.00 mL, 4.00 M).

For each kinetic run, a vial was charged with **Stock Solution A** (100 μL, 0.0200 mmol Pd/L), **Stock Solution B** (trial 3: 56 μL (0.28 mmol **1**), trial 1: 75 μL (0.40 mmol **1**), trial 2: 112 μL (0.600 mmol **1**), trial 4: 150 μL (0.801 mmol **1**), respectively), and **Stock Solution C** (200 μL, 0.800 mmol **2**) sequentially. The internal standard 1,2,4,5-tetramethylbenzene (26.8 mg, 0.200 mmol) was added to the reaction vial. Additional toluene-d$_8$ (trial 3: 144 μL, trial 1: 125 μL, trial 2: 88 μL, trial 4: 50 μL, respectively) was added to the reaction vessel to maintain an overall volume of 0.500 mL. Then, the resulting homogeneous solution was quickly transferred to a J-Young tube. The J-Young tube was inserted into the preheated NMR probe (50.0 °C) and ^{1}H NMR spectra were acquired using a pre-acquisition delay in array mode for the length of the experiment. The raw data was then processed in MestReNova (peak integrations were normalized against 1,2,4,5-tetramethylbenzene as the internal standard.) and Microsoft® Excel to determine the initial rate of the reaction. The order dependence for **1** was derived as the slope of its log (initial rate) vs. log (starting concentration of **1**) plot.

Summary of reaction rates determined from disappearance of [**1**] over time by varying the concentration of [**1**]:

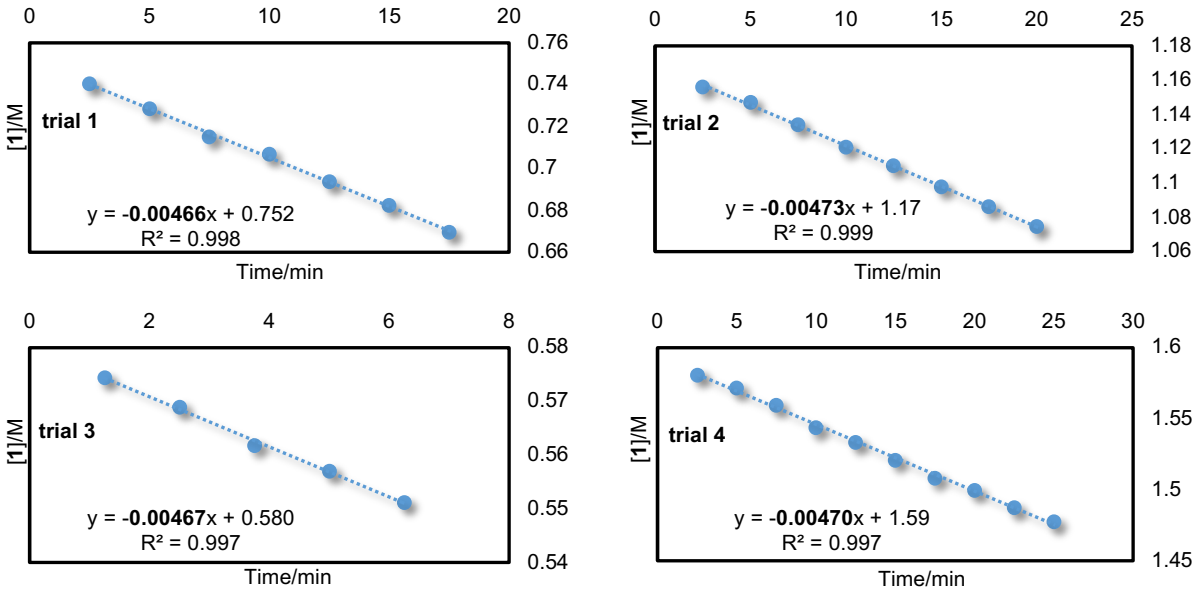

Entry	[**1**] (mol/L)	[**2**] (mol/L)	[(COD)Pd($CH_2TMS)_2$] (mol/L)	[**L**] (mol/L)	Initial Rate (M/min)
trial 1	0.800	1.60	0.0400	0.0400	0.00466
trial 2	1.20	1.60	0.0400	0.0400	0.00473
trial 3	0.600	1.60	0.0400	0.0400	0.00467
trial 4	1.60	1.60	0.0400	0.0400	0.00470

Determination of the Reaction Order in Enyne **1**:

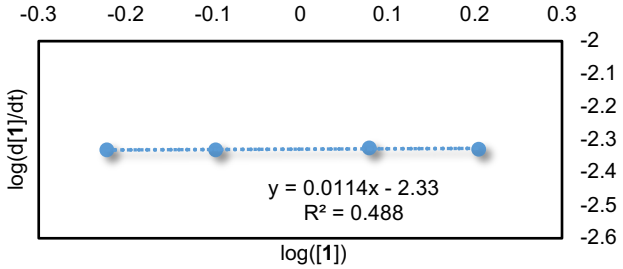

Log(*d*[**1**]/*d*t) was plotted against log[**1**] to determine the initial reaction order for **1**. The slope of the plot indicates zero-order dependence with respect to enyne **1**.

3.2 Procedure for Reaction Order Determination for C-Boron Enolate **2**

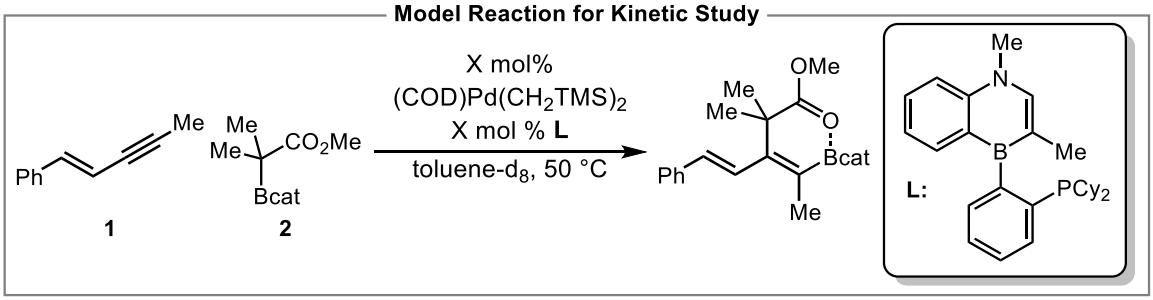

In a nitrogen-filled glovebox, (COD)Pd($CH_2TMS)_2$ (38.9 mg, 0.100 mmol) **L** (43.0 mg, 0.100 mmol) was dissolved in toluene-d_8 to prepare a **Stock Solution A** (0.500 mL, 0.200 M). Enyne **1** (427 mg, 3.00 mmol) was dissolved in toluene-d_8 to prepare a **Stock Solution B** (0.500 mL, 6.00 M). C-boron enolate **2** (880 mg, 4.00 mmol) was dissolved in toluene-d_8 to prepare a **Stock Solution C** (1.00 mL, 4.00 M).

For each kinetic run, a vial was charged with **Stock Solution A** (100 μL, 0.0200 mmol Pd/L), **Stock Solution B** (50 μL, 0.30 mmol **1**) and **Stock Solution C** (trial 5: 100 μL (0.400 mmol **2**), trial 7: 125 μL (0.500 mmol **2**), trial 6: 150 μL (0.600 mmol **2**), trial 3: 200 μL (0.800 mmol **2**), respectively) sequentially. The internal standard 1,2,4,5-tetramethylbenzene (26.8 mg, 0.200 mmol) was added to the reaction vial. Additional toluene-d_8 (trial 3: 150 μL, trial 6: 200 μL, trial 7: 225 μL, trial 5: 250 μL, respectively) was added to the reaction vessel to maintain an overall volume of 0.500 mL. Then the resulting homogeneous solution was quickly transferred to a J-Young tube. The J-Young tube was inserted into the preheated NMR probe (50.0 °C) and ^1H NMR spectra were acquired using a pre-acquisition delay in array mode for the length of the experiment. The raw data was then processed in MestReNova (peak integrations were normalized against 1,2,4,5-tetramethylbenzene as the internal standard.) and Microsoft® Excel to determine the initial rate of the reaction. The order dependence for **2** was derived as the slope of its log (initial rate) vs. log (starting concentration of **1**) plot.

Summary of reaction rates determined from disappearance of [**1**] over time by varying the concentration of [**2**]:

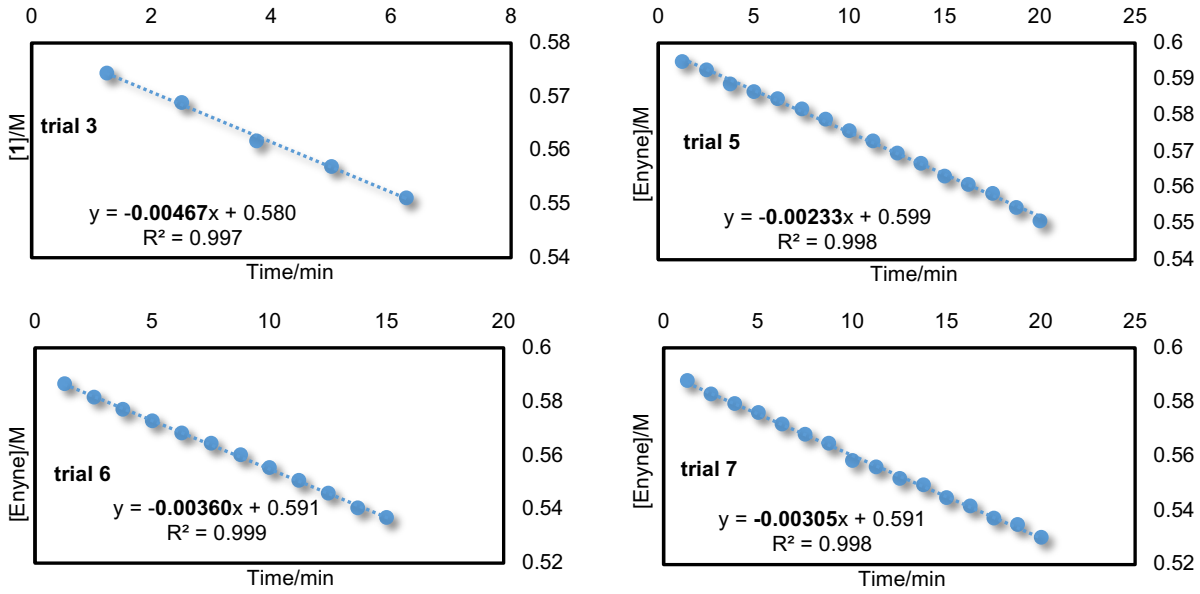

Entry	[**1**] (mol/L)	[**2**] (mol/L)	[(COD)Pd($CH_2TMS)_2$] (mol/L)	[**L**] (mol/L)	Initial Rate (M/min)
trial 3	0.600	1.60	0.0400	0.0400	0.00467
trial 5	0.600	0.800	0.0400	0.0400	0.00233
trial 6	0.600	1.20	0.0400	0.0400	0.00360
trial 7	0.600	1.00	0.0400	0.0400	0.00305

Determination of the Reaction Order in C-Boron Enolate **2**:

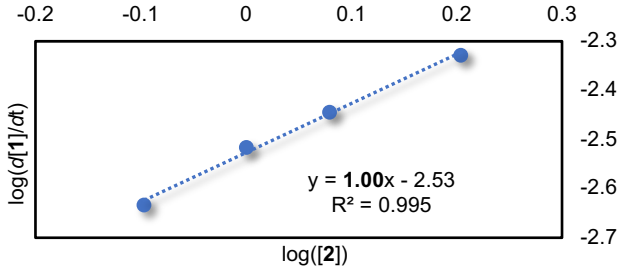

Log(d[**1**]/dt) was plotted against log[**2**] to determine the initial reaction order for **2**. The slope of the plot indicates first-order dependence with respect to C-Boron enolate **2**.

3.3 Procedure for Reaction Order Determination on **[Pd/L$_{total}$]**

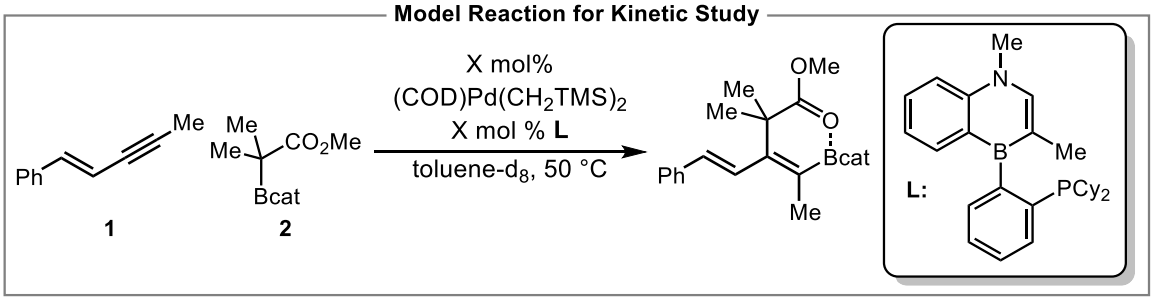

In a nitrogen-filled glovebox, (COD)Pd($CH_2TMS)_2$ (38.9 mg, 0.100 mmol) **L** (43.0 mg, 0.100 mmol) was dissolved in toluene-d_8 to prepare a **Stock Solution A** (0.500 mL, 0.200 M). Enyne **1** (427 mg, 3.00 mmol) was dissolved in toluene-d_8 to prepare a **Stock Solution B** (0.500 mL, 6.00 M). C-boron enolate **2** (880 mg, 4.00 mmol) was dissolved in toluene-d_8 to prepare a **Stock Solution C** (1.00 mL, 4.00 M).

For each kinetic run, a vial was charged with **Stock Solution A** (trial 9: 80 μL (0.016 mmol Pd/L), trial 6: 100 μL (0.200 mmol Pd/L), trial 10: 110 μL (0.220 mmol Pd/L), trial 8: 150 μL (0.300 mmol Pd/L), respectively), **Stock Solution B** (50 μL, 0.30 mmol **1**) and **Stock Solution C** (150 μL, 0.600 mmol **2**) sequentially. The internal standard 1,2,4,5-tetramethylbenzene (26.8 mg, 0.20 mmol) was added to the reaction vial. Additional toluene-d_8 (trial 8: 150 μL, trial 10: 190 μL, trial 6: 200 μL, trial 9: 220 μL, respectively) and was added to the reaction vessel to maintain an overall volume of 0.500 mL. Then the resulting homogeneous solution was quickly transferred to a J-Young tube. The J-Young tube was inserted into the preheated NMR probe (50.0 °C) and ^{1}H NMR spectra were acquired using a pre-acquisition delay in array mode for the length of the experiment. The raw data was then processed in MestreNova (peak integrations were normalized against 1,2,4,5-tetramethylbenzene as the internal standard.) and Microsoft® Excel to determine the initial rate of the reaction. The order dependence for **[Pd/L$_{total}$]** was derived as the slope of its log (initial rate) vs. log (starting concentration of **Pd/L$_{total}$**) plot.

Summary of reaction rates determined from disappearance of [**1**] over time by varying the concentration of [**Pd/L$_{total}$**]:

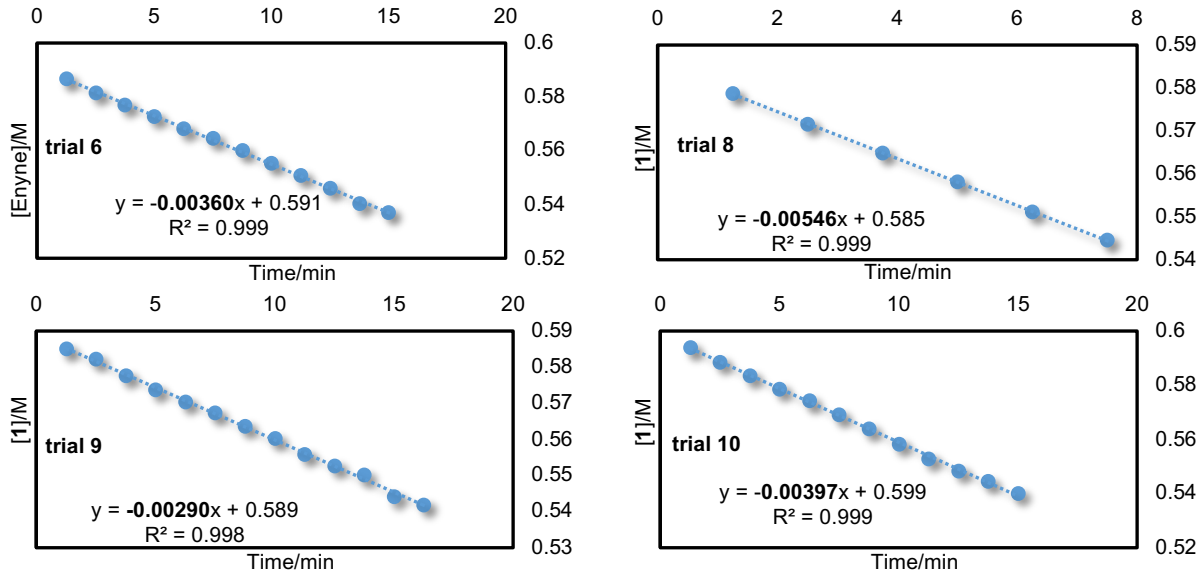

Entry	[**1**] (mol/L)	[**2**] (mol/L)	[(COD)Pd(CH$_2$TMS)$_2$] (mol/L)	[**L**] (mol/L)	Initial Rate (M/min)
trial 6	0.600	1.20	0.0400	0.0400	0.00360
trial 8	0.600	1.20	0.0600	0.0600	0.00546
trial 9	0.600	1.20	0.0320	0.0320	0.00290
trial 10	0.600	1.20	0.0440	0.0440	0.00397

Determination of the Reaction Order in [**Pd/L$_{total}$**]:

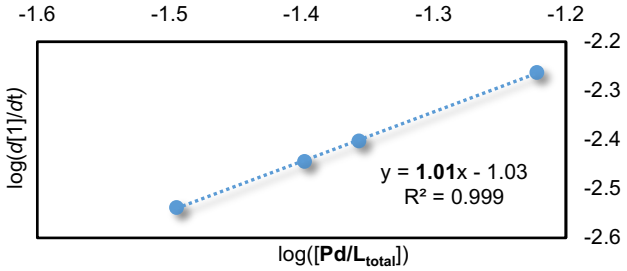

Log(d[**1**]/dt) was plotted against log[**Pd/L$_{total}$**] to determine the initial reaction order for **Pd/L$_{total}$**. The slope of the plot indicates first-order dependence with respect to enyne **Pd/L$_{total}$**.

4. Hammett Study (Scheme 5)

To study the electronic effect of the aryl group in the 1,3-enyne on the reaction rate of the carboboration reaction, we performed a Hammett analysis.

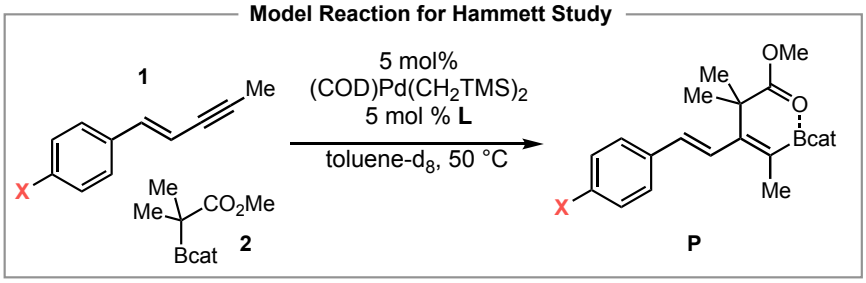

In a nitrogen-filled glovebox, $(COD)Pd(CH_2TMS)_2$ (38.9 mg, 0.100 mmol) **L** (43.0 mg, 0.100 mmol) was dissolved in toluene-d_8 to prepare a **Stock Solution A** (0.500 mL, 0.200 M). C-boron enolate **2** (880 mg, 4.00 mmol) was dissolved in toluene-d_8 to prepare a **Stock Solution B** (1.00 mL, 4.00 M).

Four oven-dried 4 mL vials were charged with 0.400 mmol of **1a (X = Cl)** (70.4 mg), **1b (X = F)** (64.0 mg), **1c (X = Me)** (62.4 mg), **1d (X = OMe)** (68.8 mg), respectively. To each oven-dried vial was added **Stock Solution A** (100 µL, 0.0200 mmol Pd/L) and **Stock Solution B** (200 µL, 0.800 mmol **2**) sequentially. The internal standard 1,2,4,5-tetramethylbenzene (26.8 mg, 0.20 mmol) was added to each of the reaction vials. Additional toluene-d_8 (150 µL) was added to each of the reaction vessels to maintain an overall volume of 0.500 mL. Then the resulting homogeneous solution was quickly transferred to a J-young tube. The J-Young tube was inserted into the preheated NMR probe (50.0 °C) and ^{1}H NMR spectra were acquired using a pre-acquisition delay in array mode for the length of the experiment. The raw data was then processed in MestreNova (peak integrations were normalized against 1,2,4,5-tetramethylbenzene as the internal standard.) and Microsoft® Excel to determine the initial rate of the reaction.

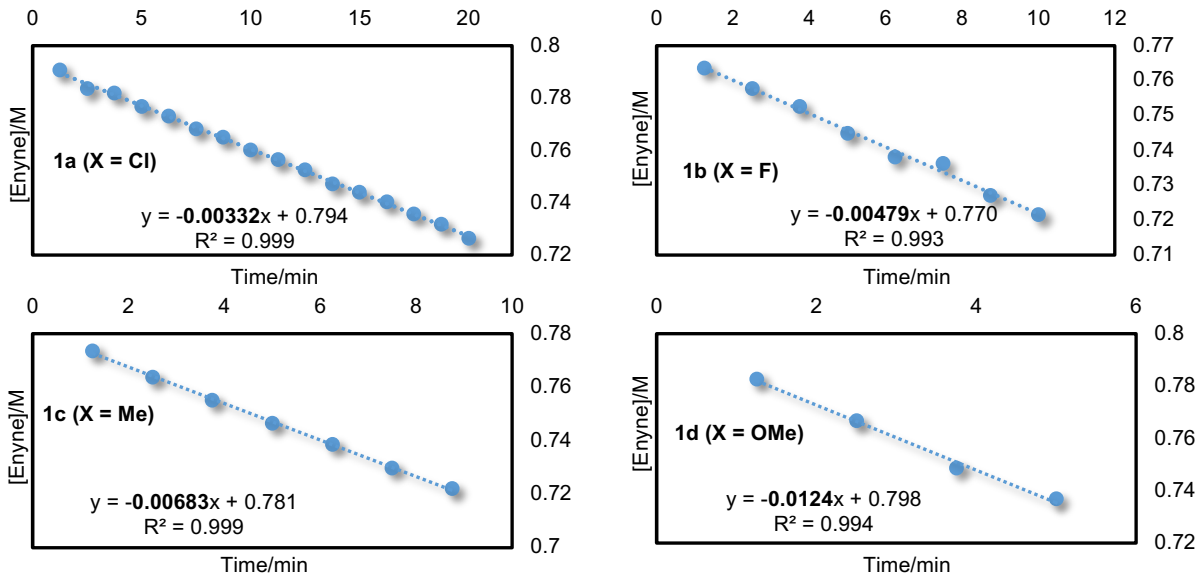

Summary of reaction rates determined from disappearance of [**1**] over time as a function of **X**:

Entry	[**1x**] (mol/L)	[**2**] (mol/L)	[(COD)Pd(CH_2TMS)$_2$] (mol/L)	[**L**] (mol/L)	Initial Rate (M/min)
1a (X = Cl)	0.800	1.60	0.0400	0.0400	0.00332
1b (X = F)	0.800	1.60	0.0400	0.0400	0.00479
1 (X = H)	0.800	1.60	0.0400	0.0400	0.00466
1c (X = Me)	0.800	1.60	0.0400	0.0400	0.00683
1d (X = OMe)	0.800	1.60	0.0400	0.0400	0.0124

Previously reported Hammett substituent constants[1] was used:

Entry	initial rate (M/min)	log([$rate_R$]/[$rate_{R=H}$])	σ_p	σ_p^+	σ_p^-
1a (X = Cl)	0.00332	-0.147	0.23	0.11	0.19
1b (X = F)	0.00479	0.0114	0.06	-0.07	-0.03
1 (X= H)	0.00466	0	0	0	0
1c (X = Me)	0.00683	0.166	-0.17	-0.31	-0.17
1d (X = OMe)	0.0124	0.426	-0.27	-0.78	-0.26

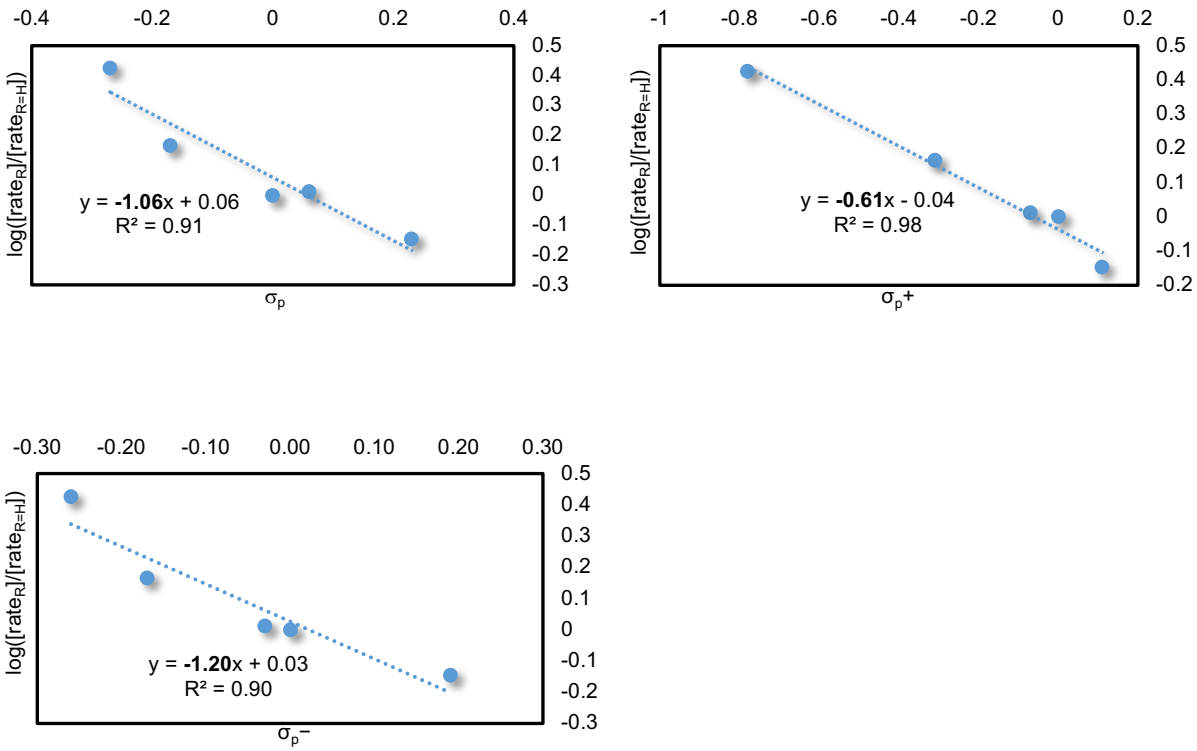

A linear fit with reported σ_p^+ constants is observed whereas a less linear fit could be obtained with σ_p or σ_p^- constants. The ρ value determined from the Hammett plot (σ_p^+) was −0.61, implying the development of some positive charge in the 1,3-enyne substrate during the transition from the resting state to the rate-limiting transition state.

Hammett Study - Product Characterization

Following the NMR kinetic analysis associated with the Hammett study, the corresponding J-Young tube containing the reaction mixture was placed in 50 °C oil bath for 12 h to complete the reaction. At the conclusion of the reaction, the mixture was allowed to cool to room temperature. The mixture was transferred to a 20 mL vial with 2 mL CH_2Cl_2 in a nitrogen-filled glovebox. A 2 mL CH_2Cl_2 solution of pinacol (591 mg, 5.00 mmol, 10.0 equiv.) and Et_3N (253 mg, 2.50 mmol, 5.00 equiv.) was added, and the resulting mixture was allowed to stir for 1 h at room temperature. Then, the mixture was concentrated *in vacuo,* and the crude residue was purified by silica gel column chromatography (2% EtOAc/Hexane to 5% EtOAc/Hexane as eluent) to afford the corresponding products as a yellow oil.

P from enyne 1a (X = Cl): 32% yield, 92:8 regioisomeric ratio.

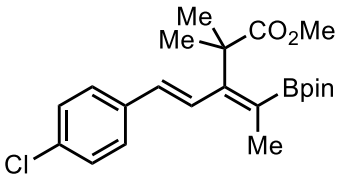

P from enyne 1a (X = Cl)

^{1}H NMR (600 MHz, $CDCl_3$) δ 7.30 – 7.23 (m, 4H), 6.59 (dd, *J* = 16.5, 1.3 Hz, 1H), 6.29 (d, *J* = 16.6 Hz, 1H), 3.62 (s, 3H), 1.85 (d, *J* = 1.2 Hz, 3H), 1.42 (s, 6H), 1.29 (s, 12H). **^{13}C NMR** (151 MHz, $CDCl_3$) δ 177.9, 147.6, 136.1, 133.1, 131.6, 128.8, 128.2, 127.5, 83.7, 52.1, 48.7, 26.8, 24.9, 19.8. (*B*-alkenyl carbon signal not observed) **^{11}B NMR** (160 MHz, $CDCl_3$) δ 31.5. **IR** ν 2977, 2934, 1729, 1605, 1510, 1496, 1455, 1372, 1327, 1301, 1268, 1247, 1210, 1174, 1143, 1107, 1075, 1033, 966, 853, 836, 814, 746, 702 cm^{-1}. **HRMS** (DART) calcd. for $C_{22}H_{31}BO_4Cl$ $[M+H^+]$: 405.19984, found 405.20039.

P from enyne 1b (X = F): 85% yield, 97:3 regioisomeric ratio.

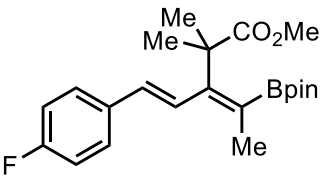

P from enyne 1b (X = F)

^{1}H NMR (600 MHz, $CDCl_3$) δ 7.35 – 7.30 (m, 2H), 7.02 – 6.96 (m, 2H), 6.53 (dd, *J* = 16.7, 1.4 Hz, 1H), 6.31 (d, *J* = 16.6 Hz, 1H), 3.63 (s, 3H), 1.87 (s, 3H), 1.43 (s, 6H), 1.30 (s, 12H). **^{13}C NMR** (151 MHz, $CDCl_3$) δ 177.9, 162.4 (d, *J* = 246.4 Hz), 147.7, 133.8 (d, *J* = 3.2 Hz), 131.7, 127.8 (d, *J* = 7.9 Hz), 127.3, 115.5 (d, *J* = 21.5 Hz), 83.7, 52.1, 48.8, 26.7, 24.9, 19.8. (*B*-alkenyl carbon signal not observed) **^{11}B NMR** (192 MHz, $CDCl_3$) δ 30.3. **^{19}F NMR** (564 MHz, $CDCl_3$) δ -114.8. **IR** ν 2978, 2934, 1730, 1600, 1508, 1459, 1372, 1330, 1296, 1262, 1229, 1144, 1077, 966, 852, 831, 813, 694, 520 cm^{-1}. **HRMS** (DART) calcd. for $C_{22}H_{31}BO_4F$ $[M+H^+]$: 389.22939, found 389.22920.

P from enyne 1c (X = Me): 88% yield, > 98:2 regioisomeric ratio.

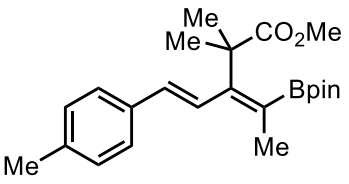

P from enyne 1c (X = Me)

^{1}H NMR (500 MHz, $CDCl_3$) δ 7.28 (d, *J* = 8.1 Hz, 2H), 7.13 (d, *J* = 7.9 Hz, 2H), 6.59 (dd, *J* = 16.5, 1.3 Hz, 1H), 6.34 (d, *J* = 16.6 Hz, 1H), 3.64 (s, 3H), 2.34 (s, 3H), 1.89 (d, *J* = 1.1 Hz, 3H), 1.45 (s, 6H), 1.32 (s, 12H). **^{13}C NMR** (126 MHz, $CDCl_3$) δ 178.0, 148.1, 137.4, 134.9, 132.8, 129.4, 126.5, 126.3, 83.6, 52.1, 48.8, 26.8, 24.9, 21.3, 19.8. (*B*-alkenyl carbon signal not observed) **^{11}B NMR** (160 MHz, $CDCl_3$) δ 31.2. **IR** ν 2978, 2930, 1732, 1511, 1459, 1372, 1331, 1297, 1264, 1212, 1192, 1145, 1079, 966, 851, 802 cm^{-1}. **HRMS** (DART) calcd. for $C_{23}H_{34}BO_4$ [$M+H^+$]: 385.25447, found 385.25597.

P from enyne 1d (X = OMe): 83% yield, > 98:2 regioisomeric ratio.

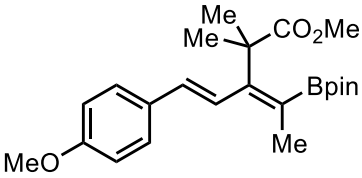

P from enyne 1d (X = OMe)

^{1}H NMR (500 MHz, $CDCl_3$) δ 7.31 (d, J = 8.7 Hz, 2H), 6.85 (d, J = 8.7 Hz, 2H), 6.49 (dd, J = 16.6, 1.2 Hz, 1H), 6.31 (d, J = 16.5 Hz, 1H), 3.80 (s, 3H), 3.63 (s, 3H), 1.88 (d, J = 1.1 Hz, 3H), 1.44 (s, 6H), 1.31 (s, 12H). **^{13}C NMR** (126 MHz, $CDCl_3$) δ 178.1, 159.3, 148.1, 132.3, 130.5, 127.5, 125.4, 114.1, 83.6, 55.4, 52.0, 48.8, 26.7, 24.9, 19.8. (*B*-alkenyl carbon signal not observed) **^{11}B NMR** (160 MHz, $CDCl_3$) δ 31.2. **IR** ν 2976, 2933, 1728, 1605,1576, 1510, 1463, 1443, 1371, 1328, 1296, 1246, 1211, 1173, 1143, 1077, 1033, 965, 916, 851, 830, 812, 771, 732, 694, 673, 647, 578, 525 cm^{-1}. **HRMS** (DART) calcd. for $C_{23}H_{34}BO_5$ [$M+H^+$]: 401.24938, found 401.24917.

5. Arrhenius Analysis and Eyring Analysis (Scheme 6)

To obtain experimental activation parameters of the carboboration reaction, we performed the Arrhenius and Eyring analysis. The reaction rate constant was obtained via initial rate kinetic analysis via ^{1}H NMR spectroscopy.

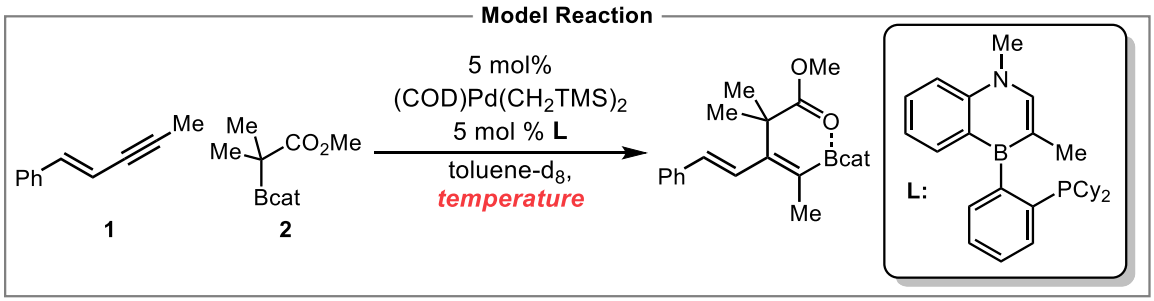

In a nitrogen-filled glovebox, (COD)Pd(CH$_2$TMS)$_2$ (38.9 mg, 0.100 mmol) **L** (43.0 mg, 0.100 mmol) was was dissolved in toluene-d$_8$ to prepare a **Stock Solution A** (0.500 mL, 0.200 M). Enyne **1** (427 mg, 3.00 mmol) was dissolved in toluene-d$_8$ to prepare a **Stock Solution B** (0.500 mL, 0.600 M). C-boron enolate **2** (880 mg, 4.00 mmol) was dissolved in toluene-d$_8$ to prepare a **Stock Solution C** (1.00 mL, 4.00 M).

For each run, a vial was charged with **Stock Solution A** (100 µL, 0.0200 mmol Pd/L), **Stock Solution B** (50 µL, 0.30 mmol **1**) and **Stock Solution C** (200 µL, 0.800 mmol **2**) sequentially. The internal standard 1,2,4,5-tetramethylbenzene (26.8 mg, 0.20 mmol) was added to the reaction vial. Additional toluene-d$_8$ (150 µL) was added to the reaction vessel to maintain an overall volume of 0.500 mL. Then the resulting homogeneous solution was quickly transferred to a J-Young tube. The J-Young tube was inserted into the preheated NMR probe (T = 25.0, 34.0 or 42.0 °C, respectively) and ^{1}H NMR spectra were acquired using a pre-acquisition delay in array mode for the length of the experiment. The raw data was then processed in MestreNova (peak integrations were normalized against 1,2,4,5-tetramethylbenzene as the internal standard.) and Microsoft® Excel to determine the initial rate of the reaction.

Summary of reaction rates determined from disappearance of [**1**] over time at different temperature:

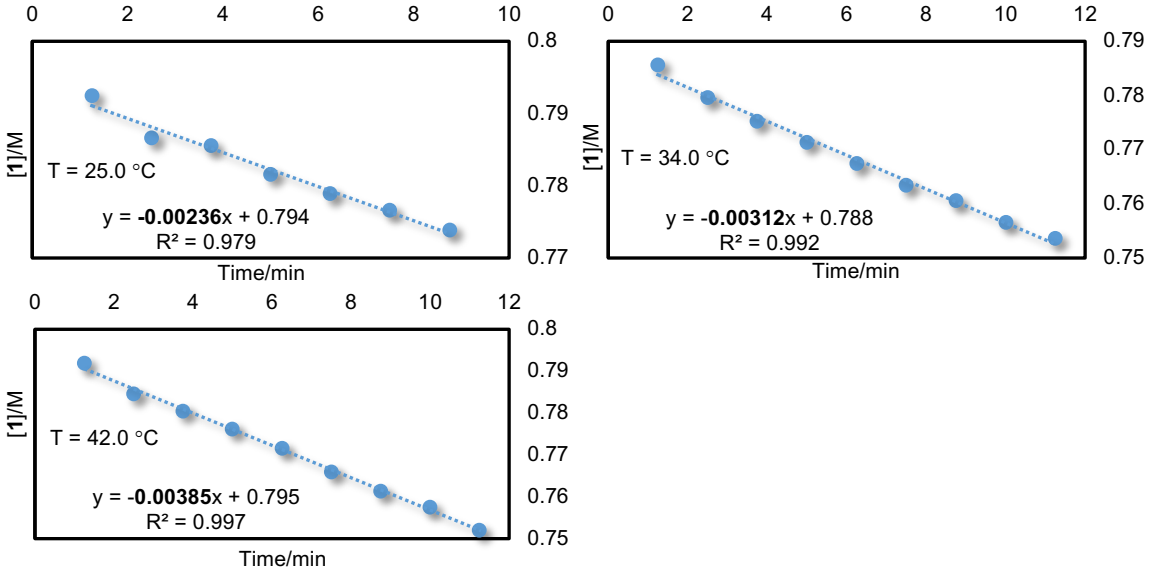

Arrhenius Analysis:

T (°C)	1/T(K^{-1})	k_{obs} (M/min)	k_{obs}(M/s)	k($M^{-1}s^{-1}$)	lnk
50.0	0.00309	0.00466	0.0000777	0.00121	–0.00671
42.0	0.00317	0.00385	0.0000642	0.00100	–0.00690
34.0	0.00326	0.00312	0.0000521	0.000814	–0.00711
25.0	0.00335	0.00236	0.0000393	0.000614	–0.00739

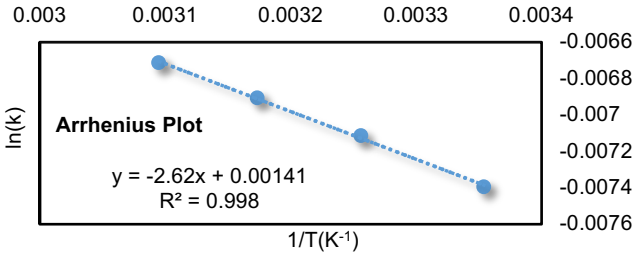

Arrhenius equation: $k=Ae^{\left(\frac{-\Delta E_a}{RT}\right)}$. Taking natural logarithm yields: $ln\ k=\frac{-\Delta E_a}{R}\cdot\frac{1}{T}+ln\ A$.

With R as the gas constant (R = 8.31441 J/K/mol) and T as the reaction temperature (T = 323.15 K), the E_a was calculated from the slope and the A was calculated from the intercept of the Arrhenius plot: E_a = 5.21 ± 0.14 kcal/mol, A =4.10 ± 0.96 $M^{-1}s^{-1}$.

Eyring Analysis:

T (°C)	1/T(K^{-1})	k_{obs}(M/min)	k_{obs}(M/s)	k($M^{-1}s^{-1}$)	Rln(kh/k_BT) (kcal·K^{-1}·mol^{-1})
50.0	0.00309	0.00466	0.0000777	0.00121	–0.0720
42.0	0.00317	0.00385	0.0000642	0.00100	–0.0723
34.0	0.00326	0.00312	0.0000521	0.000814	–0.0727
25.0	0.00335	0.00236	0.0000393	0.000614	–0.0732

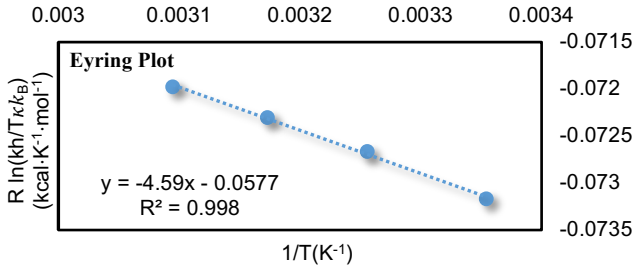

Eyring equation: $k=\frac{\kappa k_B T}{h} e^{(\frac{-\Delta G^{\ddagger}}{RT})} = \frac{\kappa k_B T}{h} e^{(\frac{-\Delta H^{\ddagger}}{RT})} e^{(\frac{\Delta S^{\ddagger}}{R})}$. Taking natural logarithm yields: $ln\frac{k}{T} = ln\frac{\kappa k_B}{h} + \frac{-\Delta H^{\ddagger}}{R} \cdot \frac{1}{T} + \frac{\Delta S^{\ddagger}}{R}$. Rearranging as: $R \cdot ln\frac{kh}{T\kappa k_B} = -\Delta H^{\ddagger} \cdot \frac{1}{T} + \Delta S^{\ddagger}$.

With R as the gas constant (R = 8.31441 J/K/mol), T as the reaction temperature (here T = 323.15 K), h as Planck's constant ($h = 6.62617 \cdot 10^{-34}$ J·s), k_B as the Boltzmann constant ($k_B = 1.380662 \cdot 10^{-23}$ J·K^{-1}) and the statistical factor κ set to 1.0, $\Delta H^{\ddagger}$ was calculated from the slope and $\Delta S^{\ddagger}$ was calculated from the intercept of the Eyring plot: $\Delta H^{\ddagger}$ = 4.59 ± 0.15 kcal/mol, $\Delta S^{\ddagger}$ = –57.75 ± 0.48 eu, $\Delta G^{\ddagger}_{323} = \Delta H^{\ddagger} - T\Delta S^{\ddagger}$ = 23.25 ± 0.22 kcal/mol.

6. BN vs CC: Ligand Performance Comparison (Scheme 7)

We compared the performance of Senphos (BN ligand) and its carbonaceous version (CC ligand) under otherwise identical condition by ^{1}H NMR analysis to obtain the 1,3-enyne concentration over time profile.

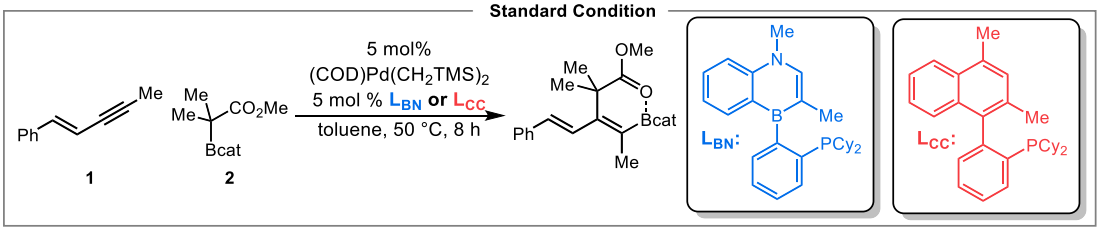

In a nitrogen-filled glovebox, to an oven-dried 4 mL vial was added (COD)Pd(CH_2TMS)$_2$ (7.8 mg, 0.020 mmol) $\mathbf{L_{BN}}$ (8.6 mg, 0.020 mmol) or $\mathbf{L_{CC}}$ (8.6 mg, 0.020 mmol) in toluene-d_8 (100 µL). The resulting mixture was allowed to stir at room temperature for 10 min before adding **1** (56.9 mg, 0.400 mmol) and **2** (176 mg, 0.800 mmol) in toluene-d_8 (100 µL). The internal standard 1,2,4,5-tetramethylbenzene (26.8 mg, 0.200 mmol) was then added to the reaction vial. Additional toluene-d_8 (150 µL) was added to the solution to maintain an overall 0.500 mL volume. The resulting homogeneous solution was quickly transferred to J-Young tube. The J-Young tube was inserted into the preheated NMR probe (T = 50 °C) and ^{1}H NMR/^{31}P NMR spectra were acquired using a pre-acquisition delay in array mode for the length of the experiment. The raw data of ^{1}H NMR was then processed in MestReNova (peak integrations were normalized against 1,2,4,5-tetramethylbenzene as the internal standard) and Microsoft® Excel to obtain the concentration of **1** over time profile. The ^{31}P NMR was processed in MestReNova to observe the formation and disappearance of the resting state Pd-enyne complex. The signal for Pd/L_{BN}-enyne complex in ^{31}P NMR persisted for ca. 4.0 hours, consistent with the reaction progress. The signal for Pd/L_{CC} complex in ^{31}P NMR persisted for ca. 1.5 hours, consistent with catalyst decomposition after 1.5 hours.

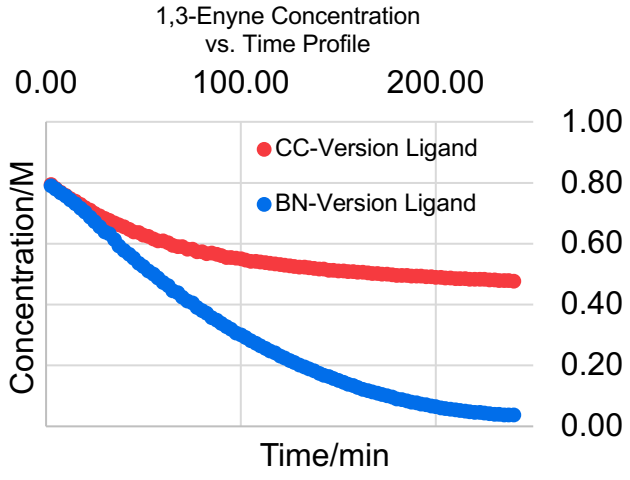

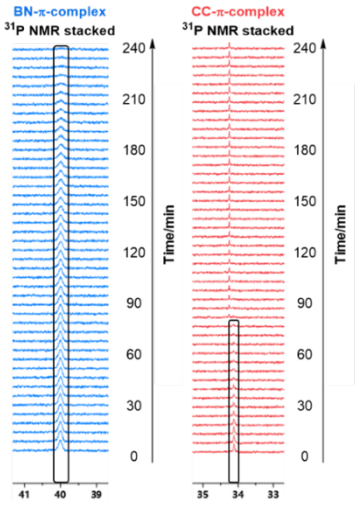

7. Computational Details (Figures 1-2)

All calculations were performed on the real systems with the Gaussian 09 package[2] and the TPSS[3] functional with D3 dispersion correction of Grimme with Becke–Johnson damping (DFT-*D3*(*BJ*))[4]. The palladium atom was described with the relativistic electron core potential SDD and associated basis set, augmented by a set of f-orbital polarization functions.[5] The 6-31G** basis set was employed for all other atoms. All stationary points involved were fully optimized by considering solvent effect (Toluene) by means of the universal Solvation Model based on solute electron Density (SMD).[6] Frequency calculations were undertaken to confirm the nature of the stationary points, yielding one imaginary frequency for transition states (TS), corresponding to the expected process, and all frequencies are positive for *minima*. The connectivity of the transition states and their adjacent *minima* was confirmed by intrinsic reaction coordinate (IRC)[7] calculations. Standard thermodynamic corrections (T = 298 K, 1 atm) have been considered to express reaction paths in terms of standard Gibbs free energies.

NBO analysis (NBO 7.0 version)[8] was used to gain more insight on the bonding situation in the Pd-enyne complex and in the transition state **TS2** associated with the *syn* outer sphere oxidative addition mechanism (O→Pd interaction in the C-B to Pd-O enolate isomerization). Stabilizing interactions (ΔE(2) in kcal/mol), determined at second order perturbation theory, have been computed to get insight on donor-acceptor interactions. Natural Localized Molecular Orbitals (NLMO) have also been determined.

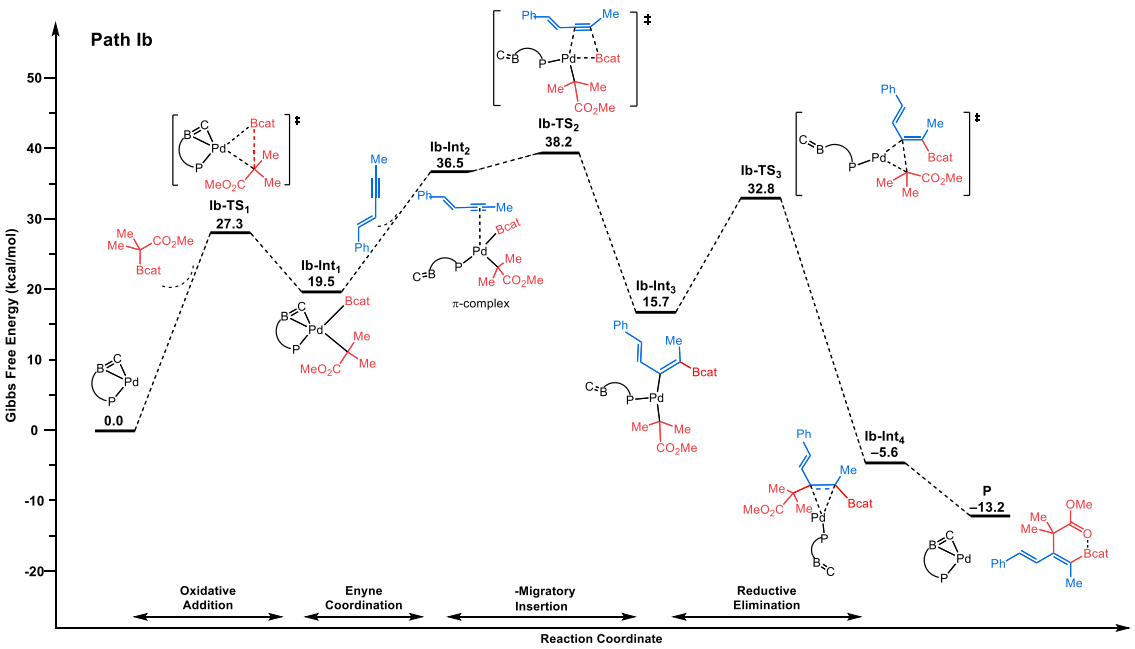

Figure S1. Energy profile (ΔG in kcal/mol) computed at SMD(Toluene)-TPSS-D3(BJ)/SDD+f(Pd), 6-31G**(other atoms) level of theory for the inner-sphere mechanism involving direct oxidative addition pathway of C-boron enolate to Pd. Path Ib is shown: Bcat moiety *trans* to phosphorus of the 1,4-azaborine-Senphos ligand.

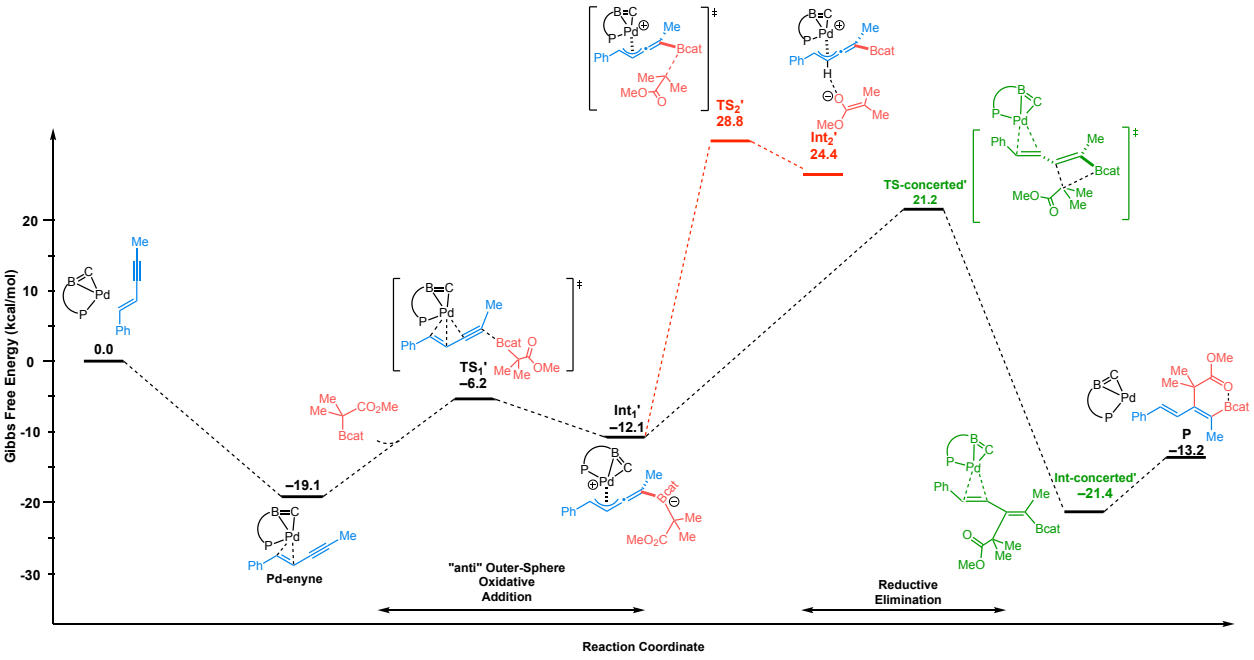

Figure S2. Energy profiles (ΔG in kcal/mol) computed at SMD(Toluene)-TPSS-D3(BJ)/SDD+f(Pd), 6-31G**(other atoms) level of theory for the *anti* outer-sphere oxidative addition mechanism, involving B-C bond cleavage without assistance of O→Pd interaction (red path). Concerted reductive elimination (green path) was also considered.

For the *anti* outer-sphere oxidative addition mechanism, starting from the π-complex, the activation barrier for the oxidation-addition step is 12.9 kcal/mol, indicating a feasible process. A η^3-Pd-allyl complex **Int$_1$'** is formed through an endergonic step from the resting state. From this oxidative addition product **Int$_1$'**, two scenarios have been investigated to explain the formation of the *cis*-carboboration product: a one-step pathway with concerted breaking of B-C bond and formation of the C-C bond through a 4-memberd ring TS (**green pathway**), or a two-step pathway involving B-C bond cleavage and then C-C bond formation (**red pathway**).The 4-membered ring transition state lies very high in energy above the π-complex ($\Delta G^{\ddagger}$: 40.3 kcal/mol, **green pathway**), which makes the process less feasible by this route. DFT calculations have also shown that the alternative stepwise pathway (**red pathway**) can be also ruled out due to the very high activation energy barrier of the B-C bond cleavage step ($\Delta G^{\ddagger}$: 47.9 kcal/mol from the resting state).

Table S1. Thermodynamic data at 25°C for transition states of the *syn*-outer-sphere oxidative addition mechanism, involving B-C bond cleavage with assistance of O→Pd interaction **TS2** or Pd-O/B-O isomerization and reductive elimination **TS3** (black path, Figure 2).

	TS2	**TS3**	**Exp**
ΔH‡(kcal/mol)	3.3	4.5	4.59 ± 0.15
ΔS‡(e.u)	-65.3	-62.3	−58 ± 1 e.u
ΔG‡(kcal/mol)	22.8	23.1	23.25 ± 0.22

Figure S3. Optimized structures (main distances in Å) for all *minima* and transition states for the proposed *syn*-outer sphere oxidative addition mechanism involving B-C bond cleavage with assistance of O→Pd interaction **TS2**, Pd-O/B-O isomerization, and reductive elimination **TS3** (black path, Figure 2).

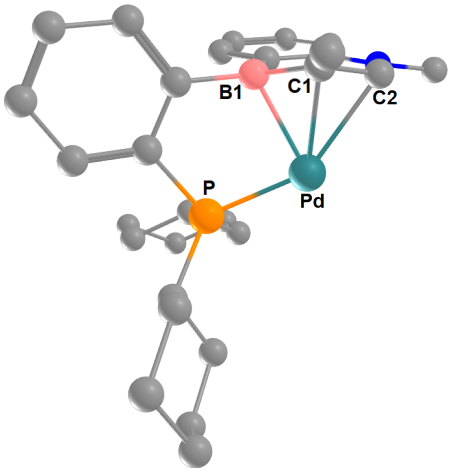

Catalyst

Pd-B[1]= 2.240 Å;
Pd-C[1]= 2.175 Å; Pd-C[2]= 2.410 Å;
Pd-P= 2.270 Å

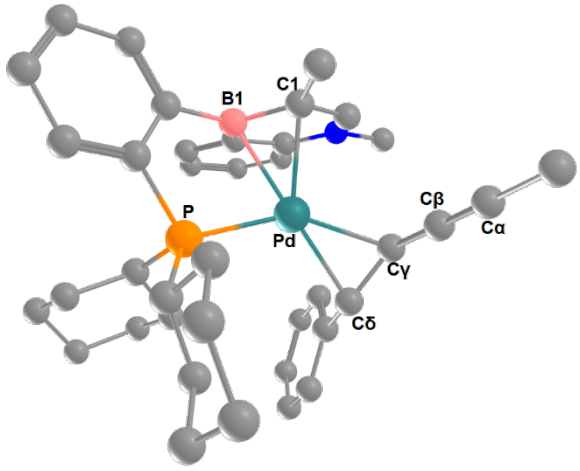

Complex π

Pd-B[1]= 2.407Å; Pd -C[1]= 2.272 Å;
Pd-P= 2.307 Å; Pd-C_{β}= 2.970 Å;
Pd-C_{γ}= 2.202Å; Pd-C_{δ}= 2.183 Å;
C_{α}-C_{β} : 1.225 Å

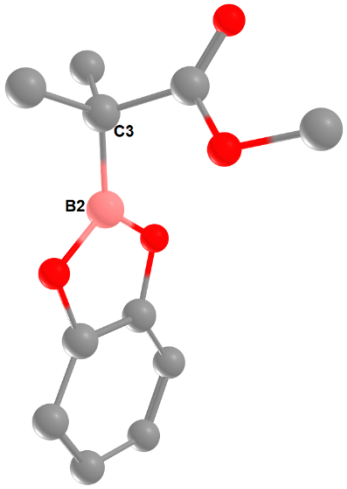

C-boron enolate

B^2-C_3= 1.578Å

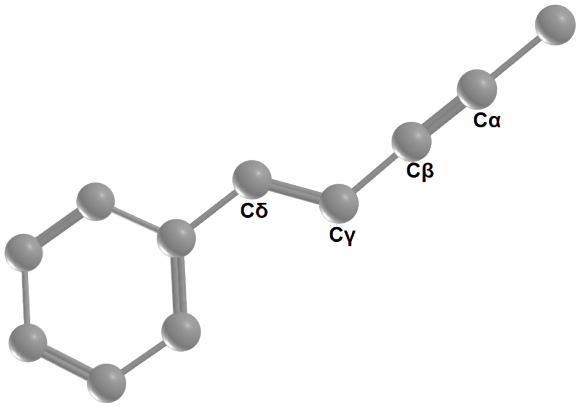

Enyne

C^{α}-C^{β} : 1.22396 Å; C_{β} - C_{γ}= 1.416 Å
C_{γ} -C_{δ}= 1.362 Å

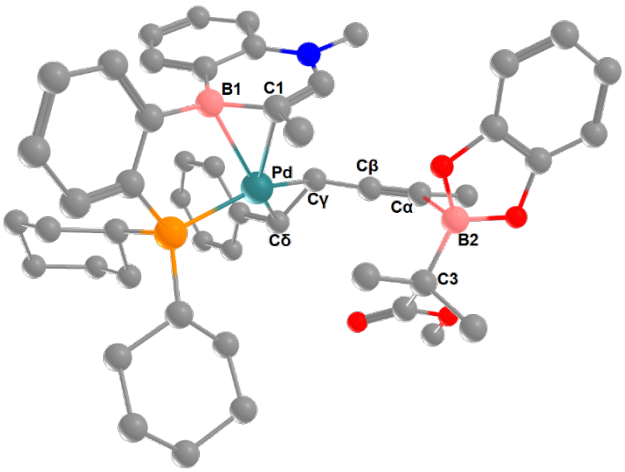

TS1

Pd-B^1= 2.366Å; Pd-C^1= 2.347 Å;
Pd-C_{β}= 3.111 Å ;
Pd-C_{γ}= 2.162Å; Pd-C_{δ}= 2.170Å ;
B^2-C_{α} = 2.291Å; C_{α}-C_{β} : 1.247 Å

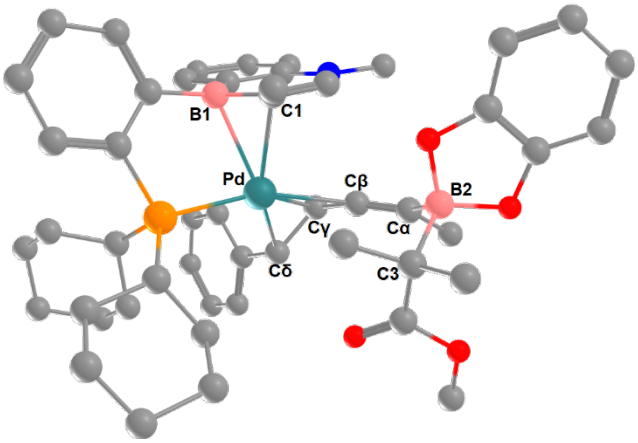

Int1

Pd-B^1= 2.425Å; Pd-C^1= 2.382 Å;
Pd-C_{β}= 2.367 Å;
Pd-C_{γ}= 2.158Å; Pd-C_{δ}= 2.215Å;
B^2-C_{α} = 1.653Å; C_{α}-C_{β} : 1.310 Å

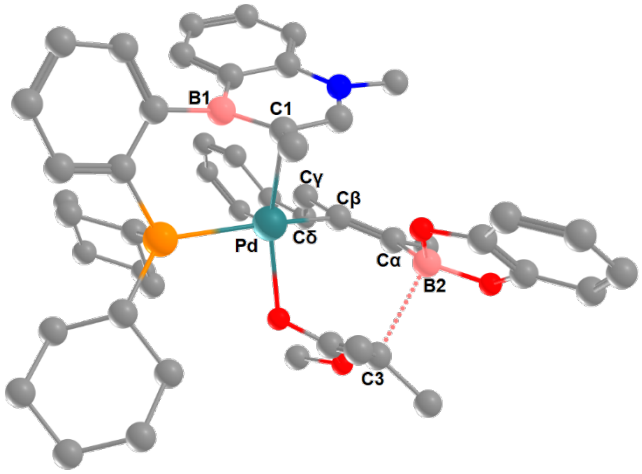

TS2

Pd-B[1]= 2.634Å; Pd-C[1]= 2.196Å;
Pd-C_{β}= 2.058 Å ;
Pd-C_{γ}= 2.706Å; Pd-C_{δ}= 3.870Å;
B^2-C_{α} = 1.563Å; C_{α}-C_{β} : 1.355Å; Pd-O= 2.138Å

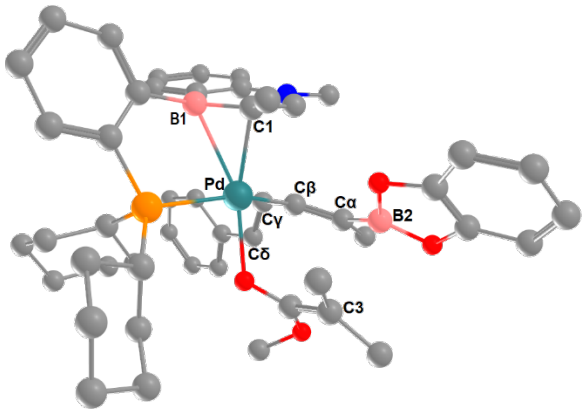

Int2

Pd-B[1]= 2.540Å; Pd -C[1]= 2.211Å;
Pd-C_{β}= 2.067 Å;
Pd-C_{γ}= 2.682Å; Pd-C_{δ}= 3.730Å;
B^2-C_{α} = 1.535Å; C_{α}-C_{β} : 1.360Å ; Pd-O= 2.130Å

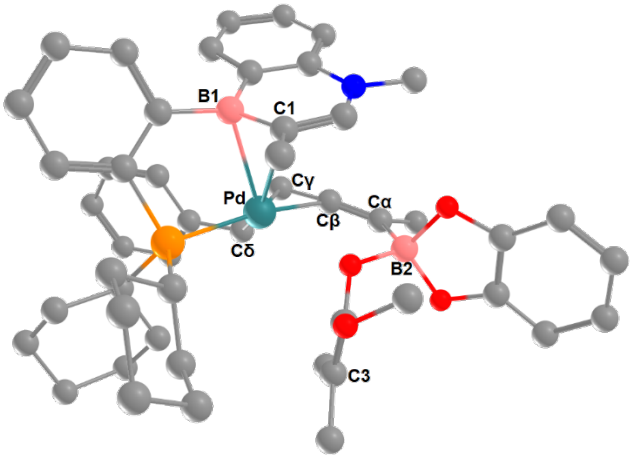

Int3

Pd-B[1]= 2.476 Å; Pd -C[1]= 2.503Å;
Pd-C_{β}= 2.181 Å;
Pd-C_{γ}= 2.168Å; Pd-C_{δ}= 2.231Å;
B^2-C_{α} = 1.630Å; C_{α}-C_{β} : 1.320Å; B^2-O= 1.517Å

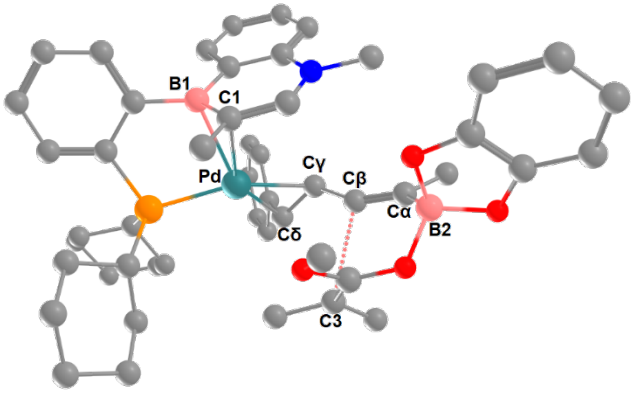

TS3

Pd-B[1]= 2.374Å; Pd -C[1]= 2.333Å;
Pd-C_{β}= 3.062 Å;
Pd-C_{γ}= 2.170Å; Pd-C_{δ}= 2.171Å;
B^2-C_{α} = 1.642Å; C_{α}-C_{β} : 1.307Å; C_{β}- C_3= 2.681Å

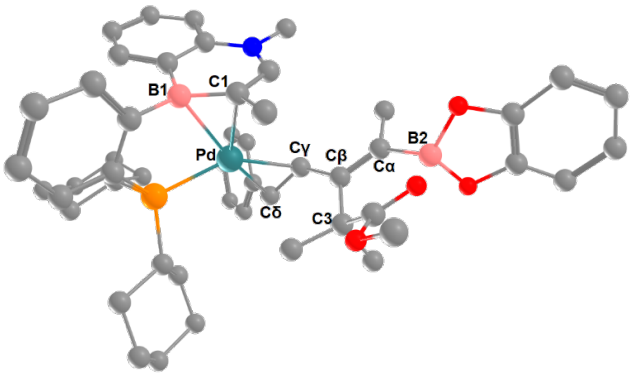

Int4

Pd-B^1= 2.361 Å; Pd -C^1= 2.264Å;
Pd-C_β= 3.153 Å;
Pd-C_γ= 2.226Å; Pd-C_δ= 2.205Å;
B^2-C_α = 1.590Å; C_α-C_β : 1.370Å ; B^2-O= 1.642Å

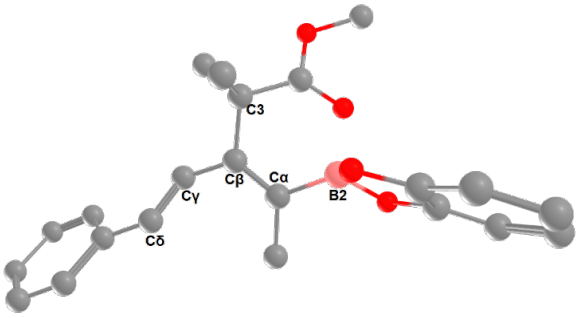

P

C_α-C_β : 1.362 Å; C_β - C_γ= 1.472 Å
C_γ -C_δ= 1.357Å;
B^2-C_α = 1.590 ; B^2-O= 1.663Å

Table S2. NBO analysis for the π-Pd-enyne complex. Stabilizing interaction ΔE(2) at the 2nd order perturbation theory in kcal/mol, associated to the donation C=C→Pd and the back-donation Pd→C=C. Plot of the associated Natural Localized Molecular Orbital (NLMO, cutoff : 0.04), with percentage of the main atoms (%) involved in each NLMO.

	NBO analysis Pd-enyne complex	
	ΔE(2)	**NLMO**
Donation $\pi_{C=C}$ **(enyne)** ⟶ **s (Pd)**	44.9	4.4% Pd 41.4%C1 46.3%C2
Back-donation d_{xy}**(Pd)** ⟶ **π*$_{C=C}$(enyne)**	35.3	78.9% Pd 8.1% C1 7.1% C2

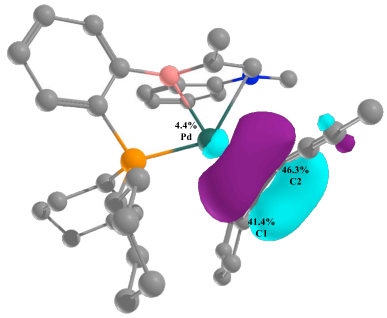

Donation
$\pi_{C=C}$ ⟶ s (Pd)

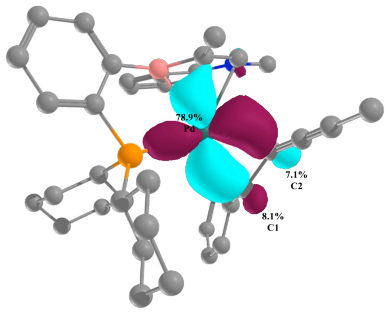

Back-donation
d_{xy}(Pd) ⟶ π*$_{C=C}$

Table S3. NBO analysis for the transition state **TS2**, associated to the *syn* outer sphere oxidative addition mechanism (C-B to Pd-O enolate isomerization). Stabilizing interaction ΔE(2) at the 2nd order perturbation theory in kcal/mol for the O→Pd interaction. Plot of the NLMO (cutoff : 0.04) associated to the main O→Pd interaction (lone pair: LP3(O)) with percentage of the main atoms (%).

	NBO analysis TS2	
	ΔE(2)	
LP1(O) → s(Pd)	12.4	
LP2(O) → s(Pd)	4.3	
		NLMO
LP3(O) → s(Pd)	13.2	5.3% Pd 77.0% O 8.6% C1 2.6% C2 0.4% C3
LP3(O) → σ^*_{Pd-C2}	14.0	
LP3(O) → π^*_{C2-C3}	1.6	

Plot of NLMO associated to LP3(O)

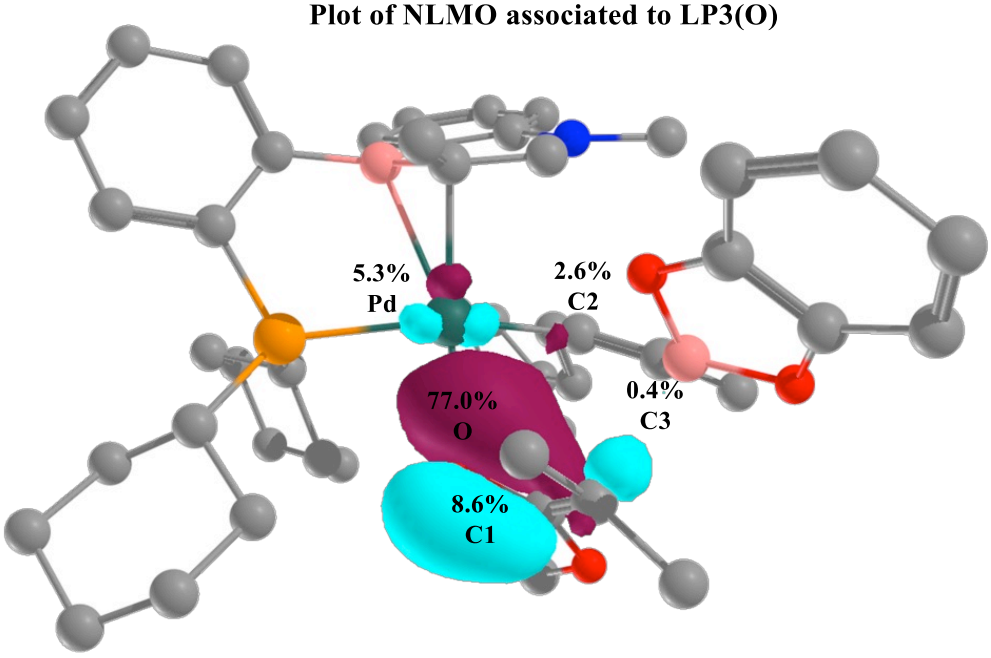

Activation Strain Model for assessing the bonding of the Pd-enyne complex

In order to understand the origin of the preferred π-alkene coordination *versus* π-alkyne coordination of the Pd-enyne complex, Activation Strain Model (ASM) calculations were carried out for the π-Alkene and the π-Alkyne Pd(0) complexes at SMD(Toluene)-TPSS D3(BJ)/SDD+f(Pd), 6-31G**(other atoms) level of theory. The Activation Strain Model (ASM) of reactivity,[9] also known as distortion/interaction model,[10] is a computational methodology to the decompose the potential energy surface, $\Delta E(\zeta)$, along the entire reaction coordinate, ζ, into the strain, $\Delta E_{strain}(\zeta)$, which is associated with the deformation of the reactants along the reaction and the interaction energy term, $\Delta E_{int}(\zeta)$, between the deformed reactants.

$$\Delta E(\zeta) = \Delta E_{strain}(\zeta) + \Delta E_{int}(\zeta)$$

The structures were divided into two fragments, Pd-catalyst and enyne. Single point energy calculations were performed for each fragment in the same geometry as the original optimized π-Alkene and π-Alkyne Pd(0) complexes. The distortion energy (ΔE_{dist}) is the energy difference between the distorted structure and optimized ground-state structure for each fragment. The interaction energy (ΔE_{int}) was calculated as the energy difference between ΔE (total) (energy difference between the optimized ground-state structures of π-Alkene and π-Alkyne Pd(0) complexes and their corresponding fragments) and the total distortion energy ($\Delta E_{strain} = \Delta E_{dist\text{-}\mathbf{Pd\text{-}catalyst}} + \Delta E_{dist\text{-}\mathbf{enyne}}$).

DFT calculations show that the alkene-coordination of the 1,3-enyne to Pd is preferred over alkyne-coordination by 9.1 kcal/mol.

The HOMO of the enyne is delocalized all around the π-system, involving C=C double bond, C≡C triple bond and phenyl ring, meaning that Pd center can interact either with double or triple bond of the enyne to form corresponding π-complexes. Analysis of the geometrical features of the two π-Pd-enyne complexes suggest that the coordination of Pd to the alkyne (Pd-C: 2.094, 2.107 Å) is stronger than to the alkene (Pd-C: 2.183, 2.202 Å) (See Figure S4). This is corroborated by the difference in the interaction energy ($\Delta\Delta E_{int}$: 5.6 kcal/mol), which is in favor of the triple bond coordination, as relevead by the Activation Strain Model (ASM) approach ($\Delta E = \Delta E_{strain} + \Delta E_{int}$) used for the two Pd(0) complexes (See Table S4). However, this stabilizing interaction is countrebalanced by the significant deformation energy of the enyne in the case of the alkyne-coordination, as attested by the deviation of the CCC bond angle ($C_\alpha C_\beta C_\gamma$:178.1° in substrate compared to $C_\alpha C_\beta C_\gamma$:152.3° and $C_{Me}C_\alpha C_{\beta:}$ 145.6 in π-alkyne complex) and by the calculated deformation energy (ΔE_{strain} : 22.5 kcal/mol in π-alkyne complex *versus* ΔE_{strain} : 9.1 kcal/mol in π-alkene) as shown by ASM results (See Table S4). We conclude that the weaker deformation energy of the enyne moiety upon coordination the double bond to the Pd center ($\Delta\Delta E_{strain}$: 15.2 kcal/mol) is responsible for the preferred Pd(0)-alkene coordination.

Figure S4. Optimized structures of enyne and π-Alkene/Alkyne Pd(0) complexes. Main distances and bond angles in Å and degrees, respectively. Relative stability (ΔG) in kcal/mol.

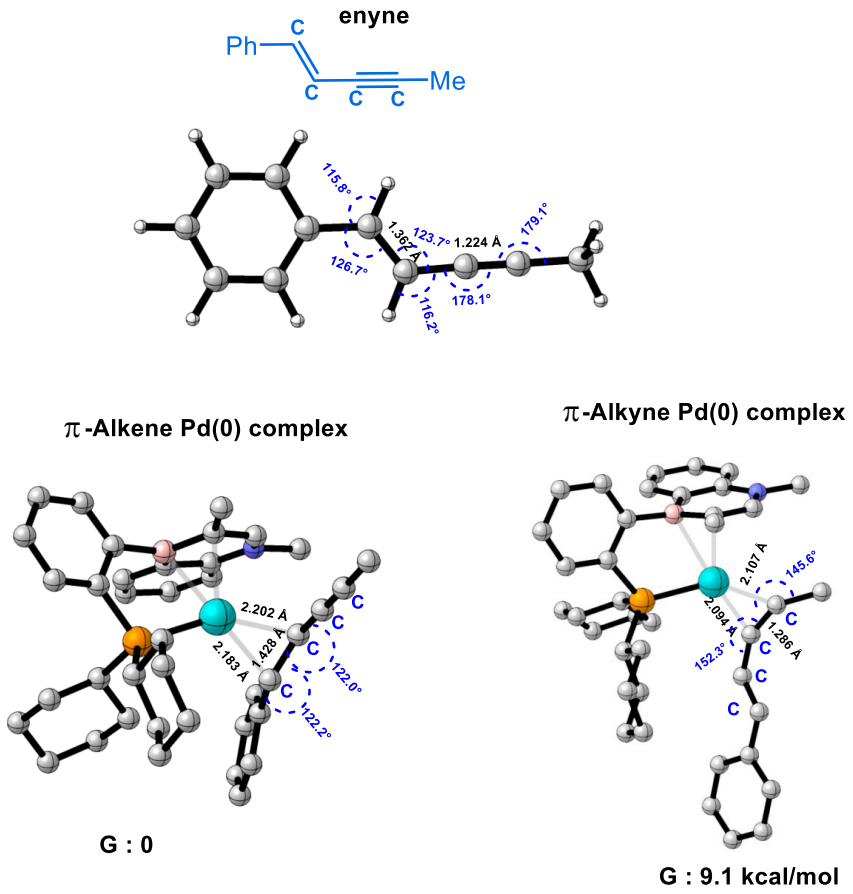

Table S4. Activation Strain Model (ASM) energies (ΔE_{strain}, ΔE_{int} in kcal/mol) for the π-Alkene and π-Alkyne Pd(0) complexes. Energy level: SMD(Toluene)-TPSS D3(BJ)/SDD+f(Pd), 6-31G**(other atoms).

	π-Alkene Pd(0) complex	**π-Alkyne Pd(0) complex**
d(Pd…C) / Å	Pd…C*γ*: 2.205Å Pd…C*δ*: 2.183 Å	Pd…C*α*: 2.107 Å Pd…Cβ: 2.095Å
Δ*E* (total)	-35.7	-26.0
ΔE_{Strain}-enyne	9.1	22.5
ΔE_{Strain}-Pd catalyst	11.2	13.0
ΔE_{Strain} (total)	20.3	35.4
ΔE_{int}	-55.9	-61.5

8. NMR Spectra

Parameter	Value
1 Origin	Varian
2 Instrument	vnmrs
3 Solvent	cdcl3
4 Temperature	25.0
5 Number of Scans	8
6 Receiver Gain	28
7 Relaxation Delay	10.0000
8 Spectrometer Frequency	599.68
9 Nucleus	1H

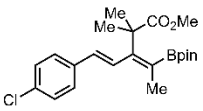

P from enyne 1a (X = Cl)

Parameter	Value
1 Origin	Varian
2 Instrument	vnmrs
3 Solvent	cdcl3
4 Temperature	25.0
5 Number of Scans	43
6 Receiver Gain	30
7 Relaxation Delay	1.0000
8 Spectrometer Frequency	150.81
9 Nucleus	13C

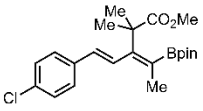

P from enyne 1a (X = Cl)

Parameter	Value
1 Origin	Varian
2 Instrument	vnmrs
3 Solvent	cdcl3
4 Temperature	25.0
5 Number of Scans	400
6 Receiver Gain	30
7 Relaxation Delay	0.0100
8 Spectrometer Frequency	160.38
9 Nucleus	11B

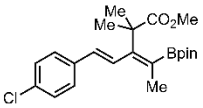

P from enyne 1a (X = Cl)

Parameter	Value
1 Origin	Varian
2 Instrument	vnmrs
3 Solvent	cdcl3
4 Temperature	25.0
5 Number of Scans	6
6 Receiver Gain	0
7 Relaxation Delay	10.0000
8 Spectrometer Frequency	599.68
9 Nucleus	1H

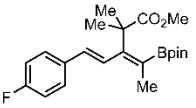

P from enyne 1b (X = F)

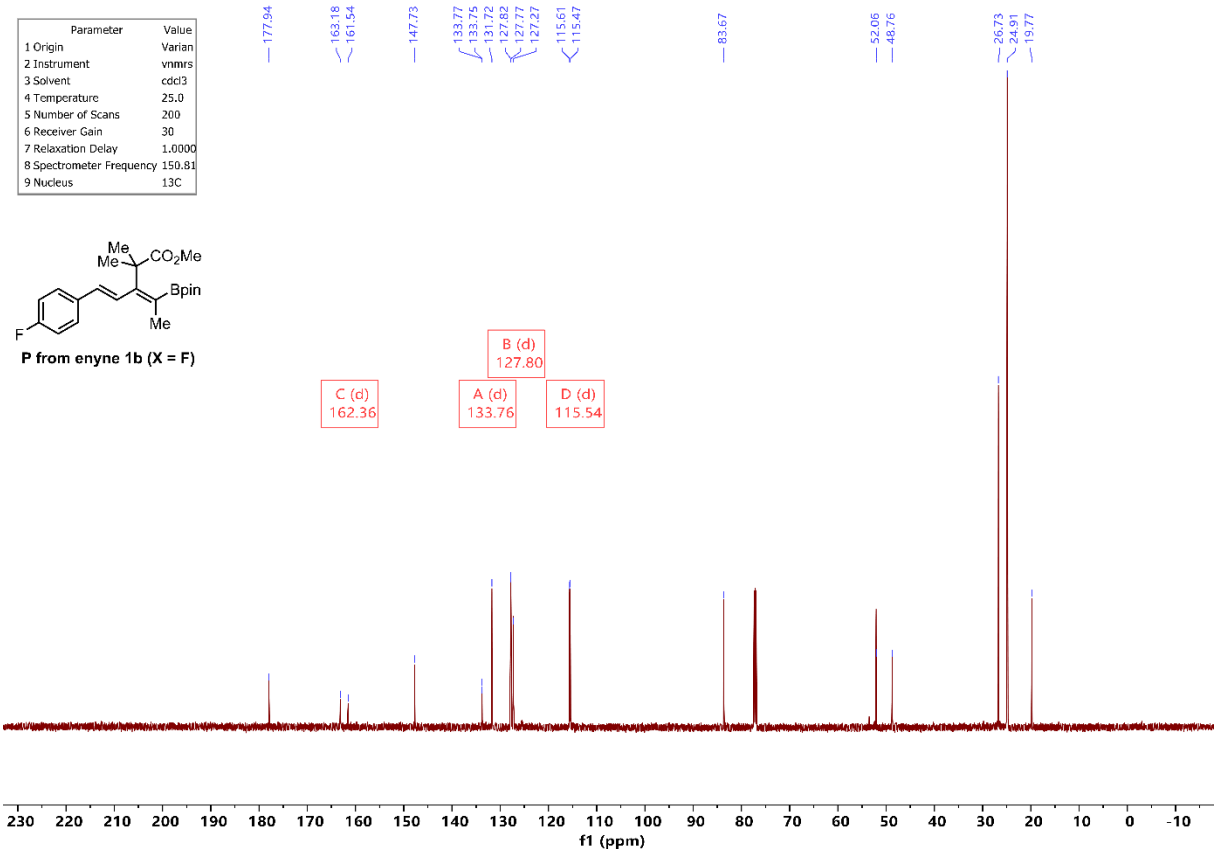
Parameter Value
1 Origin Varian
2 Instrument vnmrs
3 Solvent cdcl3
4 Temperature 25.0
5 Number of Scans 200
6 Receiver Gain 30
7 Relaxation Delay 1.0000
8 Spectrometer Frequency 150.81
9 Nucleus 13C
177.94
163.18
161.54
147.73
133.77
133.75
131.72
127.82
127.77
127.27
115.61
115.47
83.67
52.06
48.76
26.73
24.91
19.77
Me
Me
CO2Me
Bpin
Me
F
P from enyne 1b (X = F)
B (d)
127.80
C (d)
162.36
A (d)
133.76
D (d)
115.54
f1 (ppm)

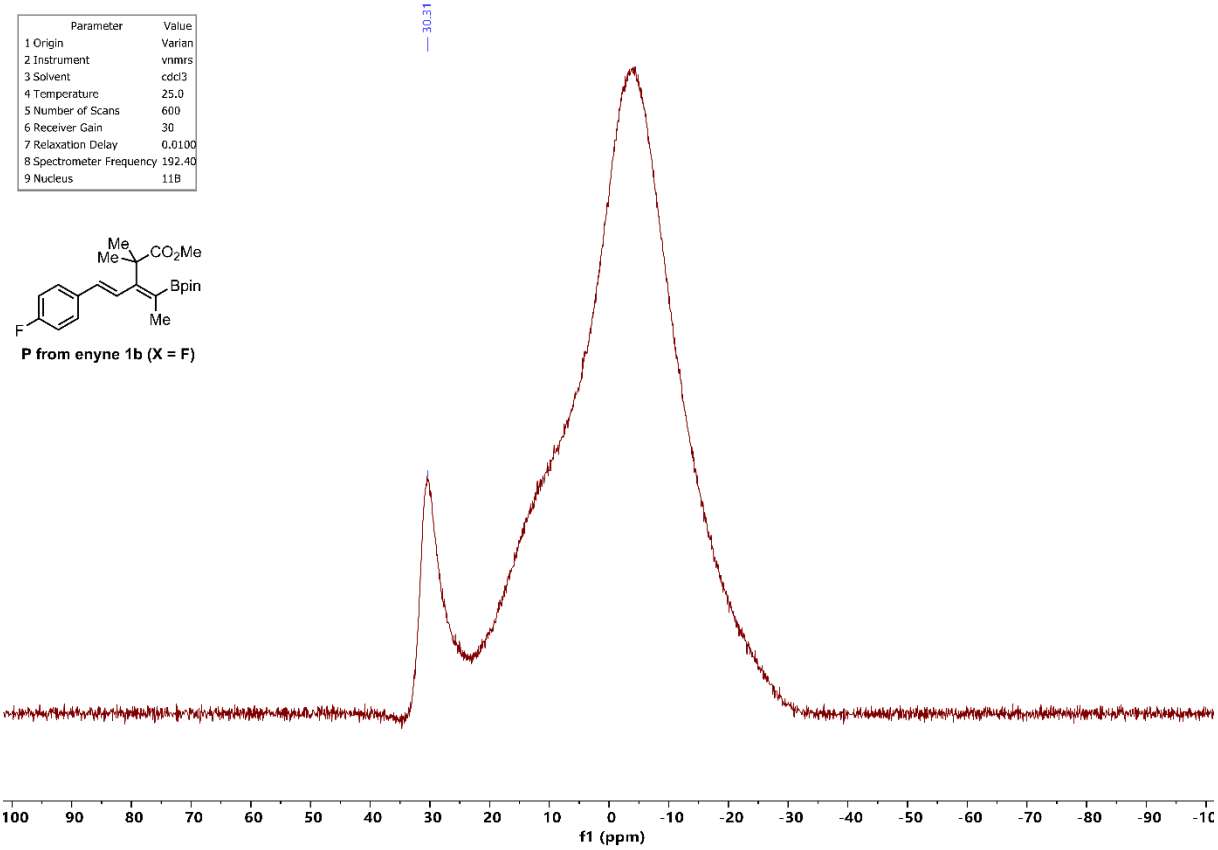
Parameter Value
1 Origin Varian
2 Instrument vnmrs
3 Solvent cdcl3
4 Temperature 25.0
5 Number of Scans 600
6 Receiver Gain 30
7 Relaxation Delay 0.0100
8 Spectrometer Frequency 192.40
9 Nucleus 11B
30.31
Me
Me
CO2Me
Bpin
Me
F
P from enyne 1b (X = F)
f1 (ppm)

Parameter	Value
1 Origin	Varian
2 Instrument	vnmrs
3 Solvent	cdcl3
4 Temperature	25.0
5 Number of Scans	16
6 Receiver Gain	46
7 Relaxation Delay	1.0000
8 Spectrometer Frequency	564.22
9 Nucleus	19F

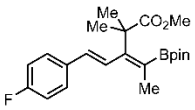

P from enyne 1b (X = F)

Parameter	Value
1 Origin	Varian
2 Instrument	vnmrs
3 Solvent	cdcl3
4 Temperature	25.0
5 Number of Scans	8
6 Receiver Gain	26
7 Relaxation Delay	10.0000
8 Spectrometer Frequency	499.88
9 Nucleus	1H

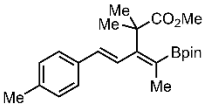

P from enyne 1c (X = Me)

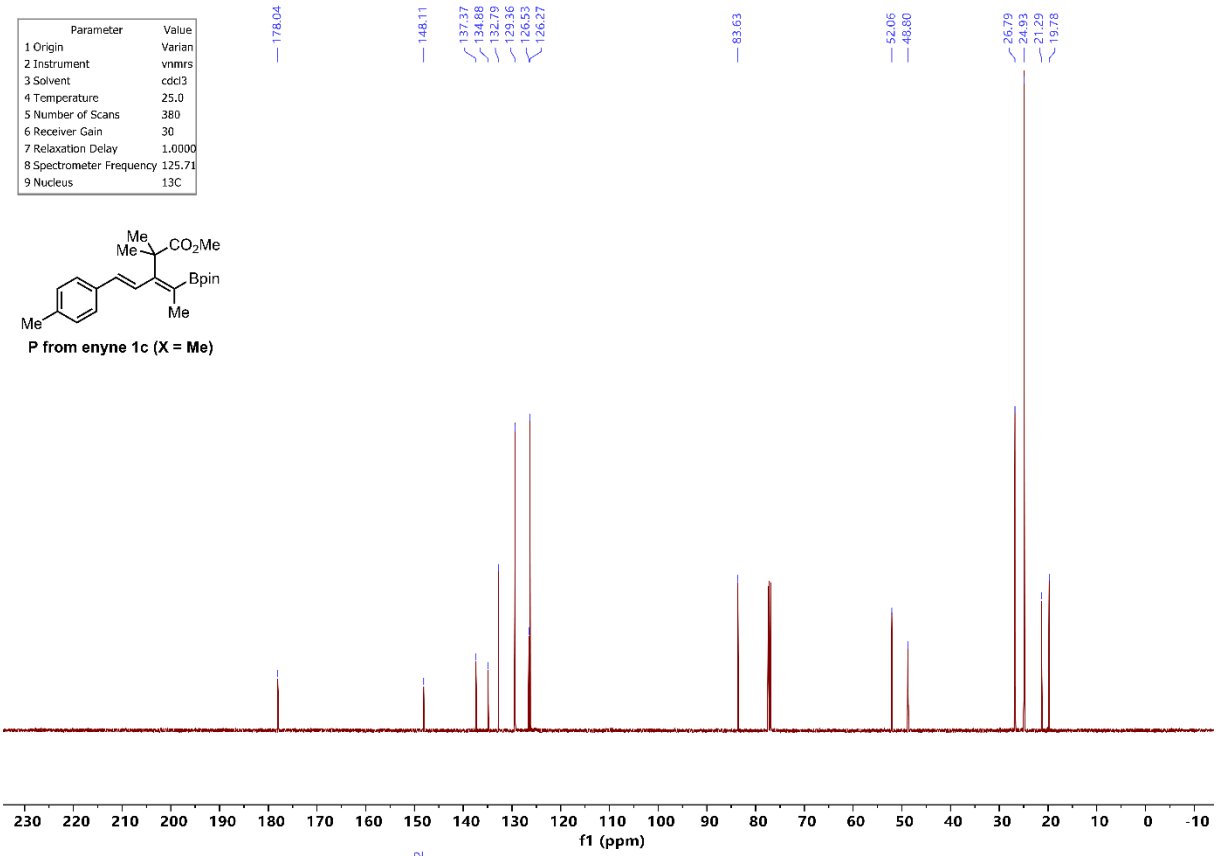

P from enyne 1c (X = Me)

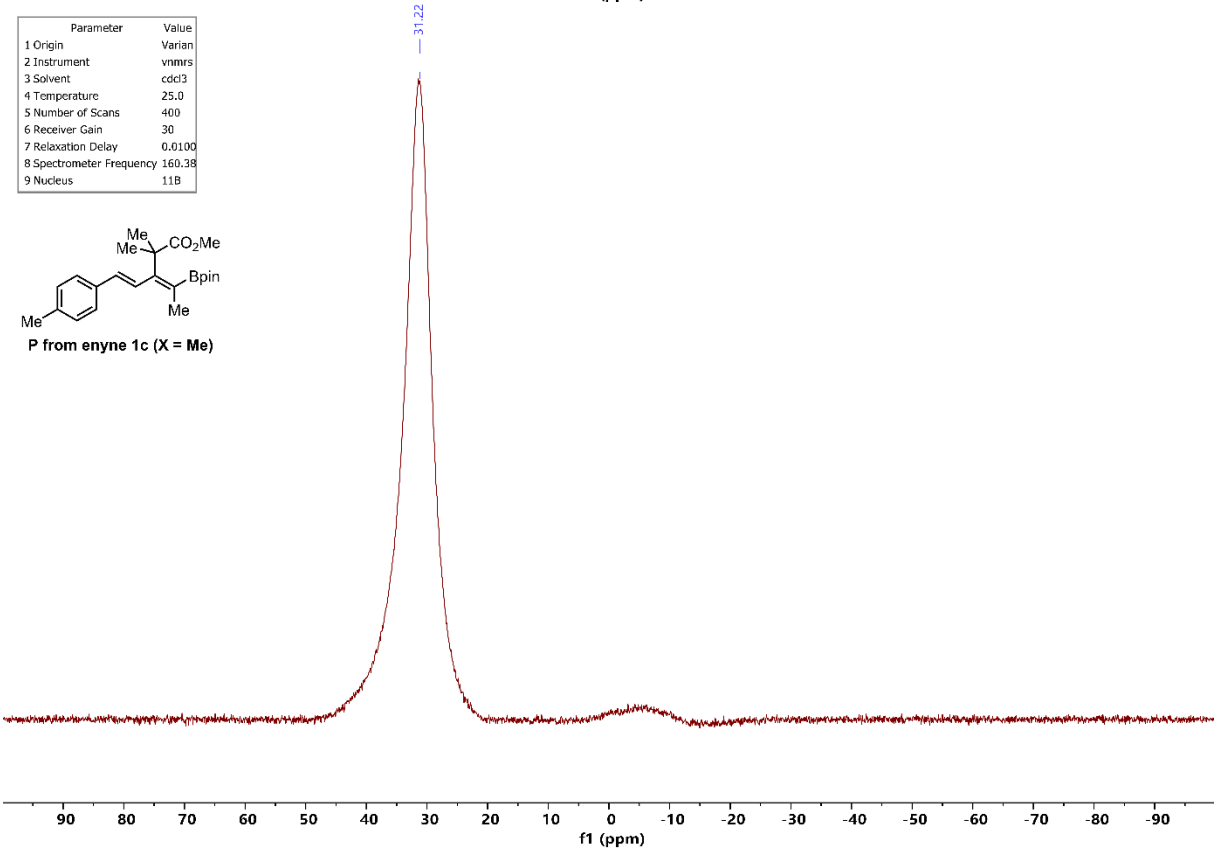

P from enyne 1c (X = Me)

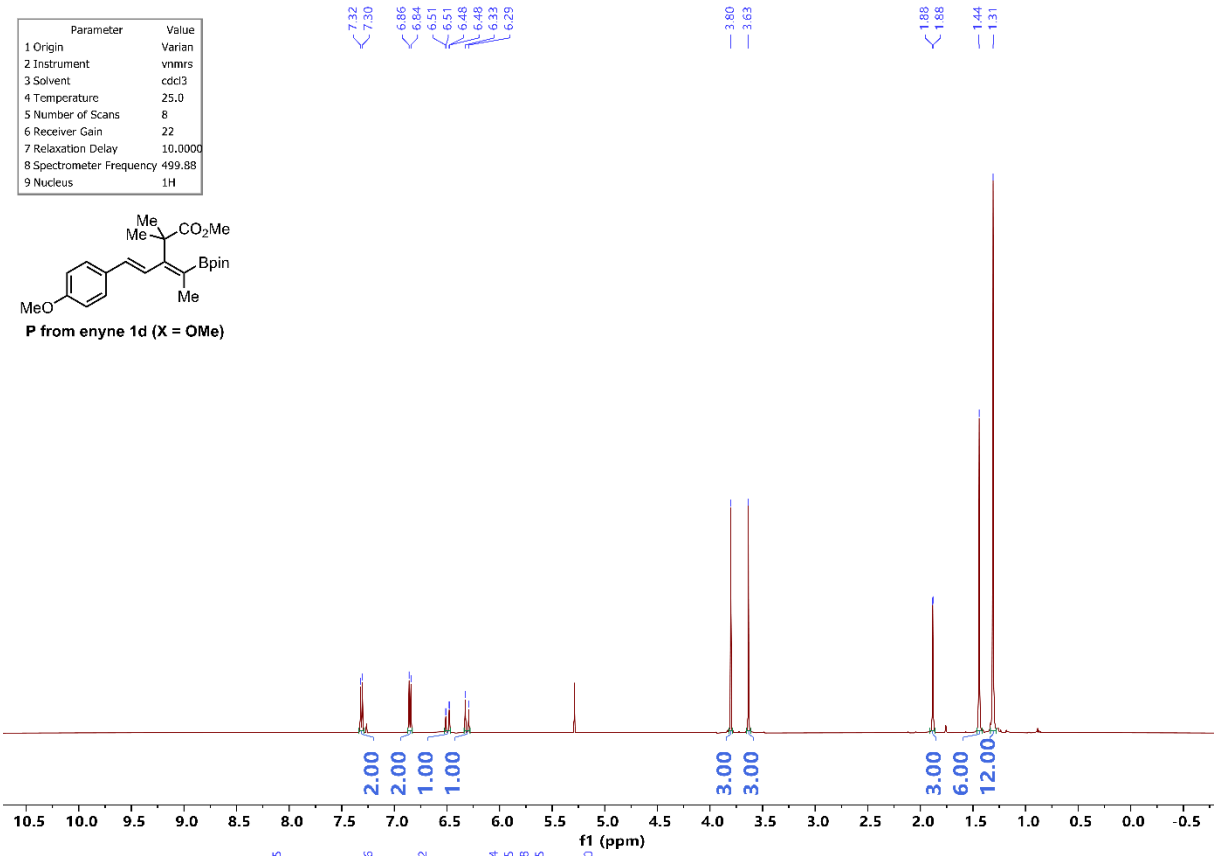
Parameter Value
1 Origin Varian
2 Instrument vnmrs
3 Solvent cdcl3
4 Temperature 25.0
5 Number of Scans 8
6 Receiver Gain 22
7 Relaxation Delay 10.0000
8 Spectrometer Frequency 499.88
9 Nucleus 1H
Me
Me
CO2Me
Bpin
Me
MeO
P from enyne 1d (X = OMe)
7.32
7.30
6.86
6.84
6.51
6.51
6.48
6.48
6.33
6.29
3.80
3.63
1.88
1.88
1.44
1.31
2.00
2.00
1.00
1.00
3.00
3.00
3.00
6.00
12.00
f1 (ppm)

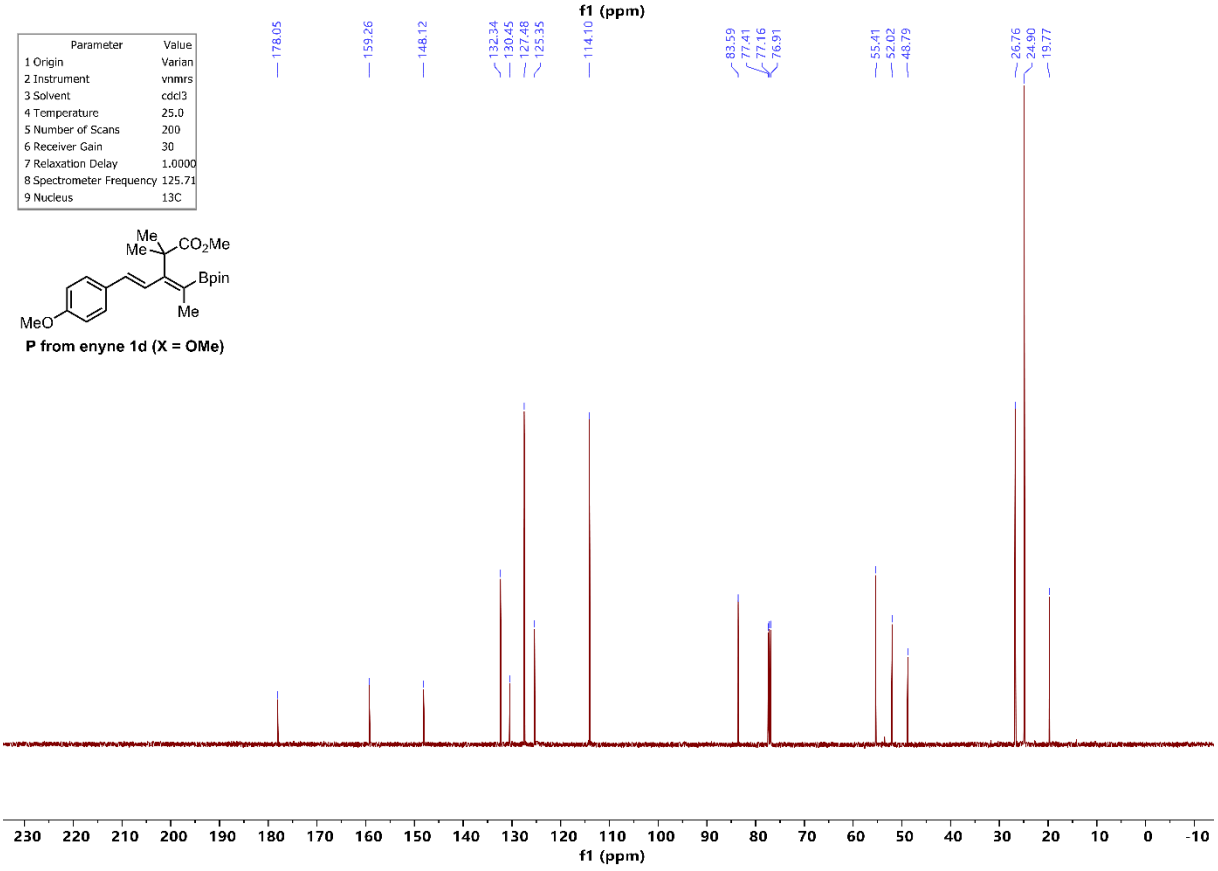
Parameter Value
1 Origin Varian
2 Instrument vnmrs
3 Solvent cdcl3
4 Temperature 25.0
5 Number of Scans 200
6 Receiver Gain 30
7 Relaxation Delay 1.0000
8 Spectrometer Frequency 125.71
9 Nucleus 13C
Me
Me
CO2Me
Bpin
Me
MeO
P from enyne 1d (X = OMe)
178.05
159.26
148.12
132.34
130.45
127.48
125.35
114.10
83.59
77.41
77.16
76.91
55.41
52.02
48.79
26.76
24.90
19.77
f1 (ppm)

Parameter	Value
1 Origin	Varian
2 Instrument	vnmrs
3 Solvent	cdcl3
4 Temperature	25.0
5 Number of Scans	600
6 Receiver Gain	30
7 Relaxation Delay	0.0100
8 Spectrometer Frequency	160.38
9 Nucleus	11B

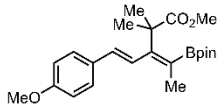

P from enyne 1d (X = OMe)

9. References

1) C. Hansch, A. Leo and R. W. Taft, *Chem. Rev.*, 1991, **91**, 165-195.
2) Gaussian 09, Revision **D.01**, M. J. Frisch, G. W. Trucks, H. B. Schlegel, G. E. Scuseria, M. A. Robb, J. R. Cheeseman, G. Scalmani, V. Barone, B. Mennucci, G. A. Petersson, H. Nakatsuji, M. Caricato, X. Li, H. P. Hratchian, A. F. Izmaylov, J. Bloino, G. Zheng, J. L. Sonnenberg, M. Hada, M. Ehara, K. Toyota, R. Fukuda, J. Hasegawa, M. Ishida, T. Nakajima, Y. Honda, O. Kitao, H. Nakai, T. Vreven, J. A. Montgomery Jr., J. E. Peralta, F. Ogliaro, M. Bearpark, J. J. Heyd, E. Brothers, K. N. Kudin, V. N. Staroverov, R. Kobayashi, J. Normand, K. Raghavachari, A. Rendell, J. C. Burant, S. S. Iyengar, J. Tomasi, M. Cossi, N. Rega, J. M. Millam, M. Klene, J. E. Knox, J. B. Cross, V. Bakken, C. Adamo, J. Jaramillo, R. Gomperts, R. E. Stratmann, O. Yazyev, A. J. Austin, R. Cammi, C. Pomelli, J. W. Ochterski, R. L. Martin, K. Morokuma, V. G. Zakrzewski, G. A. Voth, P. Salvador, J. J. Dannenberg, S. Dapprich, A. D. Daniels, Ö. Farkas, J. B. Foresman, J. V. Ortiz, J. Cioslowski, D. J. Fox, Gaussian 09 (Version A.02), Gaussian, Inc., Wallingford CT, **2009**.
3) J. Tao, J. P. Perdew, V. N. Staroverov and G. E. Scuseria, *Phys. Rev. Lett.*, 2003, **91**, 146401-146404.
4) (a) S. Grimme, J. Antony, S. Ehrlich and H. Krieg, *J. Chem. Phys.*, 2010, **132**, 154104; (b) S. Grimme, S. Ehrlich and L. Goerigk, *J. Comp. Chem.*, 2011, **32**, 1456-1465.
5) (a) D. Andrae, U. Häußermann, M. Dolg, H. Stoll and H. Preuß, *Theor. Chim. Acta*, 1990, **77**, 123-141; (b) A. W. Ehlers, M. Böhme, S. Dapprich, A. Gobbi, A. Höllwarth, V. Jonas, K. F. Köhler, R. Stegmann, A. Veldkamp and G. Frenking, *Chem. Phys. Lett.*, 1993, **208**, 111-114.
6) A. V. Marenich, C. J. Cramer and D. G. Truhlar, *J. Phys. Chem. B*, 2009, **113**, 6378-6396.
7) (a) K. Fukui, *Acc. Chem. Res.*, 1981, **14**, 363-368. (b) H. P. Hratchian, H. B. Schlegel, in *Theory and Applications of Computational Chemistry: The First 40 Years*, C. E. Dykstra, G. Frenking, K. S. Kim, G. Scuseria, Eds., Elsevier, Amsterdam, **2005**, 195.
8) (a) A. E. Reed, L. A. Curtiss and F. Weinhold, *Chem. Rev.*, 1988, **88**, 899-926; (b) J. P. Foster and F. Weinhold, *J. Am. Chem. Soc.*, 1980, **102**, 7211-7218; (c) A. E. Reed and F. Weinhold, *J. Chem. Phys.*, 1985, **83**, 1736-1740. (d) NBO 7.0 program, Glendening, E. D.; Badenhoop, J. K.; Reed, A. E.; Carpenter, J. E.; Bohmann, J. A.; Morales, C. M.; Karafiloglou, P.; Landis, C. R.; Weinhold, F. Theoretical Chemistry Institute, University of Wisconsin, Madison (2018).
9) For recent reviews, see: (a) I. Fernández, F. M. Bickelhaupt*, Chem. Soc. Rev*., 2014, **43**, 4953-4967. (b) L. P. Wolters, F. M. Bickelhaupt*, WIREs Comput. Mol.* Sci., 2015, **5**, 324-343. (c) F. M. Bickelhaupt, K. N. Houk, *Angew. Chem. Int. Ed.* **2017**, *56*, 10070; *Angew. Chem*. **2017**, *129*, 10204. (d) P. Vermeeren, S. C. C. van der Lubbe, C. Fonseca Guerra, F. M. Bickelhaupt, T. A. Hamlin, *Nat. Protoc*., 2020, **15**, 649-667. (e) I. Fernández, in Discovering the Future of Molecular Sciences (Ed.: B. Pignataro), Wiley-VCH, Weinheim, 2014, 165–187.
10) (a) D. H. Ess, K. N. Houk, *J. Am. Chem. Soc*., 2007, **129**, 10646-10647. (b) D. H. Ess, K. N. Houk, *J. Am. Chem. Soc*., 2008, **130**, 10187-10198.